Jointly Modeling the Evolution of Discrete and Continuous Traits

James D. Boyko[1]*, Brian C. O'Meara[2], Jeremy M. Beaulieu[1]

[1]Department of Biological Sciences, University of Arkansas, Fayetteville, AR, 72701, USA
[2]Department of Ecology and Evolutionary Biology, University of Tennessee, Knoxville, TN, USA

*To whom correspondence should be addressed (jboyko@uark.edu).

Running head: Jointly Modeling Discrete and Continuous Traits

Key words: rate variation, Ornstein-Uhlenbeck, hidden rates, character-dependent, character-independent, discrete character, continuous character, phylogenetic comparative methods

Contributions: J.B., B.C.O., and J.M.B. designed the study. J.D.B. led software development, J.D.B. led the simulation study, and J.D.B. led the empirical example. J.D.B. wrote the first draft, and all authors contributed to the final writing of the manuscript.

Acknowledgements: The authors thank members of the Beaulieu lab for discussion.

Data Accessibility Statement: All data and code necessary to reproduce is available on GitHub: https://github.com/jboyko/2020_houwie

Abstract

Whether modeling the evolution of a discrete or continuous character, the focal trait of interest does not evolve in isolation and require comparative methods that model multivariate evolution. Progress along these lines has involved modeling multivariate evolution of the same class of character and there are fewer options when jointly modeling traits when one character is discrete and the other is continuous. Here we develop such a framework to explicitly estimate the joint likelihood for discrete and continuous characters. Specifically, our model combines the probability of observing the continuous character under a generalized OU process with the probability of the discrete character under a hidden Markov model, linked by a shared underlying regime. We use simulation studies to demonstrate that this approach, *hOUwie*, can accurately evaluate parameter values across a broad set of models. We then apply our model to test whether fleshy and dry fruits of Ericaceae lineages are correlated with their climatic niche evolution as represented by the aridity index. Consistent with expectations, we find that dry fruits have higher rates of climatic niche evolution, that the climatic niche of fleshy fruits is more conserved, and dry fruits have a more humid climatic optimum.

A common theme in comparative biology is the detection of causal, or least mechanistic, factors that affect the evolution of quantitative characters. Questions of how plant life habit influence genome size evolution (Beaulieu et al. 2012), how substrate use alters limb length evolution (Mahler et al. 2013), or how tooth morphology slowly changes in response to habitat and diet (Toljagić et al. 2018) are all examples of testing whether evolutionary changes in a discrete variable may have altered evolutionary trajectories of a continuously varying trait. One very common phylogenetic comparative approach for these types of questions is to employ an Ornstein-Uhlenbeck (OU) model, which assumes distinct regimes, described by the evolution of a discrete character, are known completely *a priori* (e.g., Butler and King 2004; Hansen et al. 2008; Beaulieu et al. 2012), or assumes that "shifts" in regimes can be inferred directly from the distribution of the continuous trait (e.g. Ingram and Mahler 2013; Uyeda and Harmon 2014; Khabbazian et al. 2016). While these approaches are practical, the discrete trait is assumed the driving force underlying the evolution of the continuous character. However, dependence rarely flows just one way in evolution, and we suspect that as often as a discrete character causes change in the continuous character, continuous characters also influence discrete character evolution, or at the very minimum, can provide information about how they may be evolving in tandem.

Progress along these lines has mostly involved acknowledging uncertainty in the evolution of the discrete character by fitting models over a large set of stochastically generated character mappings. That is, a large set of alternative reconstructions of the discrete character are obtained completely uninformed by the continuous trait's evolution, then the likelihood of the continuous character becomes the average of the likelihoods across these maps (e.g., Revell 2012). The advantage of this approach is that there is an explicit model for how regimes change

through time, but the evolution of these regimes remains entirely independent of the continuous trait, and the probability of these regimes is not explicitly considered. For example, it is possible that the model that best fits the discrete data generates stochastic maps that does not provide a good fit to the continuous data.

A promising approach was recently described for detecting adaptive codon evolution (Jones et al 2020), where a set of maps obtained for a discrete phenotype under a standard Markov process is optimized along with parameters associated with genotype properties, thus forcing an emergent dependency between the two. Similarly, May and Moore (2020) developed a joint model for discrete and continuous characters under a state-dependent Brownian motion model. Their approach takes advantage of prior probabilities within a Bayesian framework to accommodate variation in the "background" rate of evolution in the continuous trait (i.e., rate variation across lineages that is independent of the discrete character under consideration). The novel Bayesian pipeline recently developed by Tribble et al. (2021) is the first attempt that we are aware of for jointly modeling discrete and continuous traits under an OU framework. Their approach samples discrete stochastic mappings informed by the discrete trait along with regime mappings which were informed by the continuous trait while accounting for the potential of hidden variation. While a more effective test of correlation between discrete and continuous characters, one drawback is that they do not explicitly account for the joint probability of the discrete and continuous parameter estimates together. They assume that the combination of independently estimated discrete and continuous models produces a joint estimate.

Here we develop and implement a framework that provides an explicitly joint estimate of the likelihood for a discrete and continuous character. Specifically, our model combines the probability of the continuous character given a particular regime evolving under a generalized

OU process, and the probability of that discrete regime painting obtained from an expanded set of Markov models, integrated over many regime paintings. We demonstrate how our framework, which we call *hOUwie*, can be used to test hypotheses of correlated evolution between discrete and continuous characters while also accounting for hidden character states and unobserved variation. Finally, we apply several *hOUwie* models to test the correlated dynamics of the mode of seed dispersal and climatic niche evolution and compare our results to those that did not account for the potential joint evolution of discrete and continuous variables.

Materials and Methods

The hOUwie model

Our model is composed of two processes: one describing the evolution of a discrete character and the other describing the evolution of a continuous character. To model the evolution of a single continuous character we use an Ornstein-Uhlenbeck (OU) model (Hansen 1997; Butler and King 2004; Hansen et al. 2008; Beaulieu et al. 2012; Ho and Ané 2014a). Formally, the OU process is an Itô diffusion satisfying:

$$dX(t) = \alpha(\theta(t) - X(t)) + \sigma dB(t).$$

Conceptually, this model combines the stochastic evolution of a trait through time with a deterministic component that models the tendency for a trait to evolve towards an "optimum." In this model, the value of a trait, $X(t)$, is pulled towards an optimum, $\theta(t)$, at a rate scaled by the parameter α. The optimum, $\theta(t)$, is a piecewise constant on intervals and takes values in a finite set $\{\theta_i\}$. This can represent the set of "selective regimes", "regimes", or Simpson's "adaptive zones" (Cressler et al. 2015), though it is consistent with a variety of true underlying microevolutionary models (Hansen 2014). Additionally, random deviations are introduced by

Gaussian white noise $dB(t)$, which is distributed as a normal random variable with mean zero and variance equal to $\sigma^2 dt$. Thus, σ^2 is a constant describing the rate of stochastic evolution away from the optimum. We use the set of extensions introduced by Beaulieu et al. (2012) and implemented in the R package *OUwie*, which allows for multiple primary optima $\theta(t)$ in which both the pull strength (α) and the rate of stochastic evolution (σ^2) can vary across the phylogeny. However, the algorithm used to calculate the likelihood described in Beaulieu et al. (2012) involves a computationally costly matrix inversion procedure. Here we implement a linear-time computation of the likelihood of Gaussian trait models following (Ho and Ané 2014a). To do this, we first transform the phylogeny such that its variance covariance matrix, V, is 3-point structured. We can write the variance covariance matrix of the untransformed phylogeny as $V = D_u \tilde{V} D_u$, where following Beaulieu et al. (2012) and Ho and Ané (2014),

$$\tilde{V}_{ij} = \sum_{\gamma=1}^{\kappa(i,j)} \frac{\sigma^2_{ij,\gamma}}{2\alpha_{ij,\gamma}} (\mathrm{e}^{2\alpha_{ij,\gamma} s_{ij,\gamma}} - e^{2\alpha_{ij,\gamma} s_{ij,\gamma-1}}),$$

$$\text{and, } D_u = e^{\sum_{\gamma=1}^{\kappa(i)} \alpha_{i,\gamma}(s_{i,\gamma} - s_{i,\gamma-1})},$$

where, s_γ is the distance from the root to the beginning of the selective regime (γ) for the κ number of selective regimes along the path from the root to the last common ancestor of i and j, $\kappa(i,j)$, or from the root to the terminal tip $i, \kappa(i)$. Our transformed phylogeny now has a variance covariance matrix $\tilde{V}_{ij}$ and diagonal matrix D_u. We can then calculate the quadratic quantities and determinant of V (Ho and Ané 2014a). The probability of our continuous trait is given by

$$log(P(X|\, D, z, \vartheta, \psi)) = n \log(2\pi) + \log(det(V)) + \frac{P'V^{-1}P - 2P'V^{-1}Q + Q'V^{-1}Q}{2},$$

where n is the number of tips in the phylogeny (ψ), P is the continuous trait value of each species, and Q is the expected value of each species given the continuous trait model calculated

following equation (11) of Beaulieu et al. (2012), D is the discrete character data, z is a particular regime mapping, and ϑ are the parameters of the *hOUwie* model.

Next, we describe the calculation of the probability of the underlying regime structure, γ, that is the joint probability of discrete characters (D) and stochastic mapping (z). This calculation is analogous to the pathway likelihood of Steel and Penny (2000). Recently, May and Moore (2020) suggested that the joint probability of a regime structure and the discrete character is the product of the probabilities of exponentially distributed waiting times. By this definition, branch lengths are the sum of waiting times. But, when we calculate the probability of starting and ending a branch in state *i*, the likelihood of a regime structure was unaffected by the number of transitions (Supplemental Materials), even though the maximum likelihood estimate should be zero transitions (O'Meara 2008). We suspect this is an issue of treating the probability density functions independently, when their convolution is required (i.e., an integral to express the amount of overlap of one function as it is shifted over another), because the time of the second transition depends on the timing of the first as well as the total branch length available. Ultimately, the effect of this inaccuracy in the May and Moore (2020) calculation is that the number of transitions has no influence on the probability of a branch's state reconstruction and that the sum of the joint probabilities will be greater than the marginal probability (for further details, and R code necessary to demonstrate these issues, we refer readers to the Supplemental Materials).

To calculate the probability of discrete characters (D) and stochastic mapping (z) we instead use an approximation. Our approximation relies on a finite number of degree-2 internodes and uses the standard Chapman-Kolmgorov equation to calculate the probabilities of beginning in a particular state i and ending in state j (Pagel 1994) and is identical to a joint

probability of a set of state reconstructions (Yang 2006). As the number of internodes increase, the amount of time between nodes decreases and the approximation improves (Rao and Teh 2013). The joint probability of a regime structure and the discrete character *i*

$$P(D, z|Q, \psi) = P(x_0|Q, \psi) \prod_{\ell=1}^{n-1} P(z_\ell|Q, T_\ell),$$

where $\mathbf{Q}$ the instantaneous rate matrix ($\mathbf{Q} \in \vartheta$), ψ is the phylogeny, $P(x_0|\mathbf{Q}, \psi)$ is the root state probability (Pagel 1994; Yang 2006; Maddison et al. 2007), n is the number of external nodes (tips), internal nodes, and internodes (degree-2 nodes) summed, ℓ indicates a particular branch, $P(z_\ell|\mathbf{Q}, T_\ell) = e^{\mathbf{Q}T_\ell} \mathbb{1}_\gamma$, where $\mathbb{1}_\gamma$ is an indicator function which ensures that we only use the probability of states indicated by the specific the regime mapping instead of summing over all possible state combinations. The continuous character probability requires the discrete state(s) to be defined along the entire branch, thus we place transitions halfway between any two nodes.

For each set of parameters evaluated during the maximum likelihood search, a set of possible mappings of discrete states and continuous regimes are generated to evaluate the discrete and continuous likelihoods. Ideally, we would calculate the likelihood by summing across all possible reconstructions (note that we want the sum across the reconstructions, not the single reconstruction with highest likelihood). The number of such reconstructions is very large,

$$n_{\text{states}}^{(2*\text{number of taxa}-2)(1+\text{number of degree two internodes per edge})},$$

which is particularly daunting as the sum must be calculated anew for every unique examined set of parameter values as part of search. We found in early work where we did look at this exhaustively that a few mappings made up the vast majority of the total likelihood, so we set up the analysis to focus on calculating total likelihood given the highest probability mappings.

To do this, we first approximate the conditional state probabilities at nodes. The conditional state probability, unlike the more common marginal reconstruction or joint state reconstruction (Pupko et al. 2000; Felsenstein 2004; Yang 2006), calculates the probability that a node has a particular state value conditioned only on the observations of its descendants. For a particular focal node, we calculate the probability of the observing all pairwise descendant values given the OU model parameters, integrated over all possible rootward node states, and observed tipward discrete states (Fig. 1). Although this is only an approximation of the conditional state probabilities, it proves to be an essential improvement over the typical procedure of sampling many stochastic maps based solely on the discrete process. Next, the conditional probabilities of states at nodes are sampled starting with the root. Once the root is sampled, descendent states are sampled based on both the conditional ancestral values and the sampled ancestral state. This is achieved by multiplying the conditional probability of the node states by the probability of starting in the sampled rootward ancestral value and ending in any of the tipward states (the latter is calculated using familiar matrix exponentiation methods; e.g., Pagel 1994). Finally, under usual stochastic mapping procedures we would use rejection sampling (Nielsen 2002; Rao and Teh 2013) to simulate a path between the sampled rootward and tipward nodes. However, for increased computational efficiency, we opt to place transitions at pre-defined internodes. After nodes and internodes are sampled in step two, mappings are evaluated to ensure consistency with the discrete model (i.e., impossible transitions do not occur) and branches are painted based on the sampled nodes with transitions occurring half-way between nodes (and remember that a single edge may have multiple internodes placed on it).

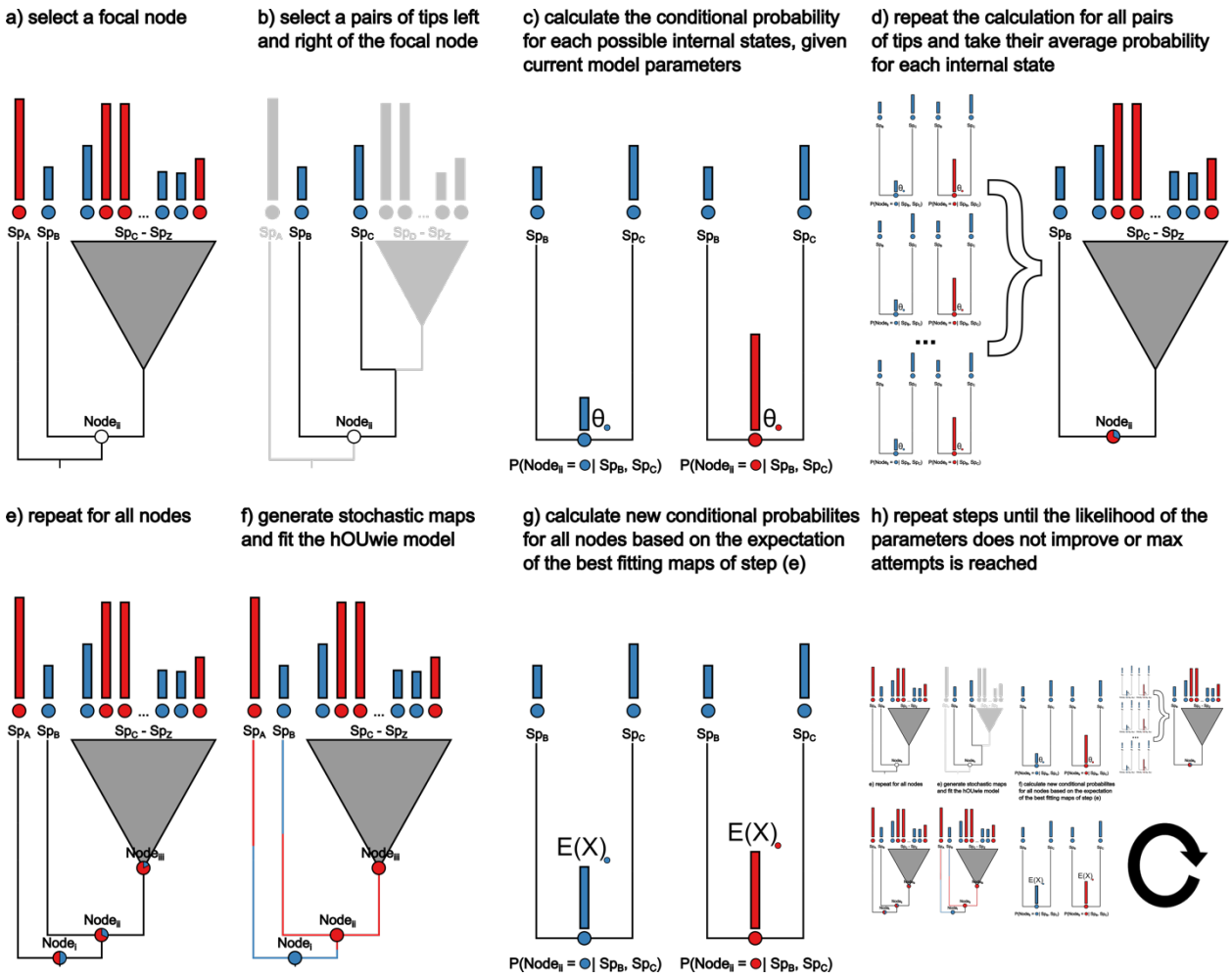

Figure 1. A visual representation of the algorithm underlying the calculation of conditional node probabilities and the adaptive sampling procedure. The goal of the procedure is to produce underlying regime paintings well suited to both the discrete and continuous character. a) select the focal node for which we will be calculating the joint conditional probabilities of the discrete and continuous characters. b) on each side of the node we select a pair of tips. c) the conditional probability of the observed discrete and continuous character is calculated for each discrete regime state with an ancestral continuous value equal to θ of that regime state. d) the conditional probability of the focal node is calculated as the average probability of each regime state for all pairs of observed tips. e) the conditional probabilities are calculated for all internal nodes. This can be turned off within hOUwie by setting the sample_nodes argument to false. f) A stochastic map is generating using forward simulation rejection sampling. g) adaptive sampling uses the highest joint probability of previously generated underling regimes to generate a set of ancestral continuous character values. This differs from previous ancestral values because instead of assuming the value θ for each regime state, it calculates the expected value given the root state and regime mapping for that particular node. h) we repeat steps d) through g) until the joint likelihood of the set of underlying regimes does not improve.

Our function for the joint probability of a continuous and a discrete character is,

$$P(X, D|\vartheta, \psi) = \sum_{z} P(X|\, D, z, \vartheta, \psi) P(D, z|\vartheta, \psi),$$

where summing over all generated maps (z), $P(X|\, D, z, \vartheta, \psi)$ is the probability of the continuous character (X) given the discrete character data (D), mapping (z), hOUwie parameters (ϑ), and phylogeny (ψ). $P(D, z|\vartheta, \psi)$ is the joint probability of the discrete character data (D) and stochastic mapping (z) given the *hOUwie* parameters (ϑ) and phylogeny (ψ).

The hOUwie model space

Our simulation studies examined 22 possible *hOUwie* model structures for a binary discrete character, although the possible number of models is significantly higher because any number of discrete characters and states can be modeled together. For the discrete component of the model, we assumed that transitions between the observed characters were equal. We constrained transitions between hidden states to be the same for observed states, but this constraint can be relaxed if desired. The continuous model structures allowable in *hOUwie* are a generalized form of those allowed in *OUwie* and now include models in which only α varies (OUA), only σ^2 varies (OUV), and combinations of an OU and BM process (OUBM1 and OUBMV). We note that the OUBM1 model within *hOUwie* differs from The Ornstein–Uhlenbeck Brownian-motion (OUBM) model presented in Hansen et al. (2008) and Bartoszek et al. (2012) since the latter models are of multiple continuous characters, rather than different processes describing the same continuous character.

The potential model structures range from completely character-dependent to character-independent. Character-dependent (CD) models are models in which *any* continuous OU parameter differs between observed discrete state, whereas character-independent models (CID)

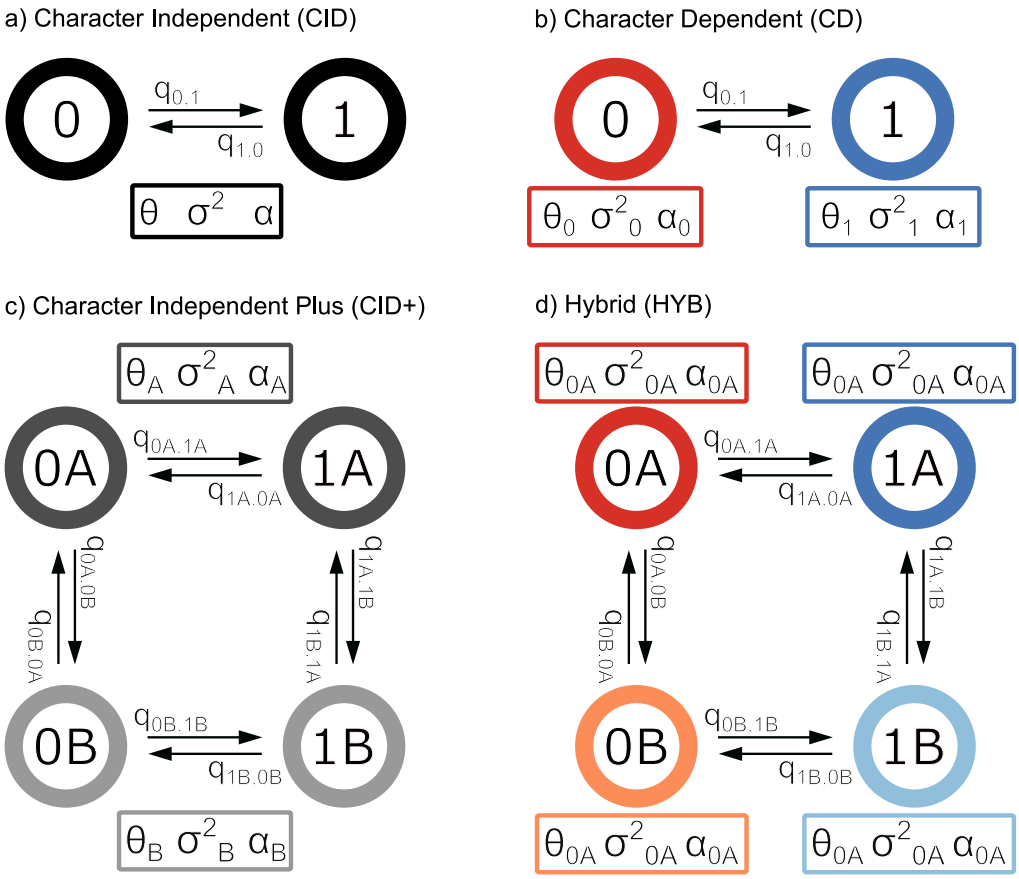

Figure 2. A state-transition diagram describing the model classes allowable in hOUwie. Each panel is comprised of observed discrete states 0 and 1 with possible hidden states A and B. Transitions between states are described with the q parameter. Continuous model parameters appear in a box below the states they describe, and their association is displayed with a subscript specific to that state. a) A simple character independent model in which the two observed states do not influence the continuous character which will have the same θ, σ^2, α throughout the phylogeny. b) A character dependent model in which the continuous character depends on the discrete character by virtue of θ, σ^2, α being associated with a particular observed discrete state. c) A character independent model with rate heterogeneity. The two observed states (0 and 1) are not directly linked to the continuous character. However, the continuous character is still allowed to have multiple θ, σ^2, α describing its evolution, but these parameters are associated with hidden states A and B. d) A hybrid model in which each combined observed and hidden state is allowed to have its own θ, σ^2, α. Under this model, the continuous character is linked to both character dependent differences (parameters associated with 0 and 1) and character independent differences (A and B). Though this diagram shows a binary observed and hidden character, either can have more states (up to 26 states for each in theory, though few datasets will have enough power to estimate the necessary number of parameters).

229 test whether observed discrete states can be described by the same OU parameters. There are two

230 types of character-independent model (Fig. 2). First, character-independent models include

structures where there are no differences between any OU parameters. Under this model the entire evolutionary history of the clade can be described by a single α, σ^2, and θ (Fig. 2a). To combat this unrealistic assumption we introduce a character-independent model which allows for differences in the OU parameters to depend upon an unobserved hidden state (CID+) and has been shown to correct for the bias towards detecting correlation (Boyko and Beaulieu 2022). This addition allows for heterogeneity within the evolutionary process without the necessity of it being linked to a focal trait (Fig. 2c). In total we examine 22 unique model structures (2 CID, 10 CD, and 10CID+).

Simulation study

For each of the 22 *hOUwie* model structures, we simulated 50 datasets for phylogenies of 25, 100, and 250 taxa for a total of 3300 unique datasets. Phylogenies were pure birth phylogenetic trees with $\lambda = 1$, rescaled tree height to 1, and the root state was fixed to state 1. The parameters used to generate a phenotypic dataset depend on the structure of the generating model. For example, an OUM model and OU1 model can have identical $q_{ij}, \alpha,$ and σ^2, but they must differ in θ or else OUM will collapse into OU1. The simulating parameters were chosen to match Beaulieu et al. (2012) with $q_{ij} = 0.1, \alpha_1 = 3, \alpha_2 = 1.5, \sigma_1^2 = 0.35, \sigma_2^2 = 1, \theta_1 = 2,$ and $\theta_2 = 0.75$ (Figure 3). Once a phylogeny and phenotypic dataset were simulated, we fit our models to assess parameter estimation accuracy and model selection power. Although this represents a small subset of the potentially vast parameter space available to OU models, the behavior of these models has been thoroughly characterized and thus we chose parameters within the range of typical identifiability (Beaulieu et al. 2012; Ho and Ané 2014*a*; Cressler et al. 2015). Additionally, because *hOUwie* uses a variable number of mappings, we evaluate changing the

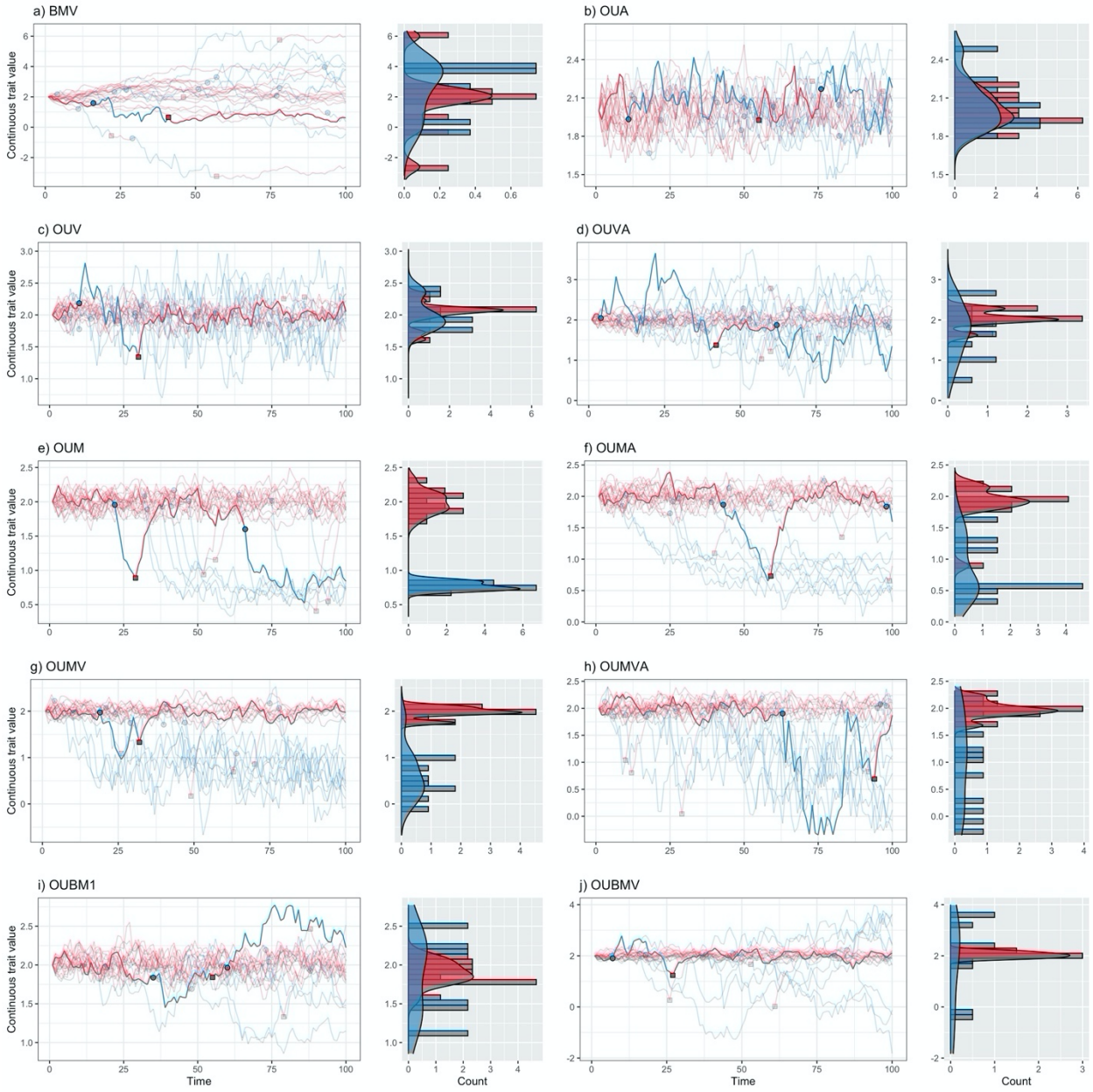

Figure 3. A visual representation of binary discrete character *hOUwie* model types. Discrete time forward simulations are conducted starting in the red state and the distribution of the continuous character is plotted on the right as a histogram and density plot. Each line represents a continuous character value at some time. Transitions occur at colored points and each line is colored by the current discrete state. 100 time-steps are simulated with the same parameters as our simulation study ($q_{ij} = 0.1, \alpha_1 = 3, \alpha_2 = 1.5, \sigma_1^2 = 0.35, \sigma_2^2 = 1, \theta_1 = 2,$ and $\theta_2 = 0.75$). The highlighted line was randomly chosen from the set in which at least one discrete state transition occurred.

number of stochastic maps. We fit each model using 25, 100, and 250 stochastic mappings per likelihood evaluation. Each dataset was evaluated using the true generating model, a BM1, an

OU1, and either the character-dependent or character-independent counterpart to the generating model. For example, if the data were simulated under a character-dependent OUM model where the value of θ_1 and θ_2 depend on the observed character, a character-independent OUM model would also be fit as part of the model set. Under the CID+ OUM model, a variable θ is still allowed, but it is unlinked to the focal character and thus should provide a more reliable character independent null hypothesis than BM1 or OU1 (Beaulieu and O'Meara 2016; Uyeda et al. 2018; May and Moore 2020; Boyko and Beaulieu 2022).

The impact of climatic variables on seed dispersal

For sedentary organisms, such as plants, dispersal is mainly limited to a brief stage of their life cycle and mediated mainly through the movement of seeds (Levin et al. 2003). Generally, the expectation is that seeds dispersed by frugivores are going to be dispersed to environments more like their parents' environment, whereas abiotically dispersed seeds are likely to be more erratic in their dispersal patterns (Schupp 1993; Westoby et al. 1996). Furthermore, it has been proposed that adaptations for frugivorous dispersal is linked to tropical and subtropical biomes, because in these warmer and wetter habitats, large trees create shady environments where competition for light is more important. A shadier habitat then imposes a selective pressure for larger seeds because more nutrients are needed for germination and initial survival (Foster and Janson 1985). However, the evolution of larger seeds comes with a tradeoff as they have a significantly lower dispersal potential (Howe and Smallwood 1982). Thus, we might expect that the climatic variables of a habitat influence the probability of transitioning between abiotic and biotic modes of dispersal, with transition rates from abiotic to biotic being greater in less arid environments.

Here we use dry or fleshy fruit morphology as a proxy for abiotic or biotic seed dispersal (Lorts et al. 2008) to evaluate three predictions outlined in Vasconcelos et al. (2021), but specifically measuring the aridity index. First, we expect that the climatic optima for fleshy fruits will be more humid compared to dry fruits ($\theta_{\text{dry}} < \theta_{\text{fleshy}}$). Second, we expect that dry fruits will have faster rates of climatic niche evolution ($\sigma^2_{\text{dry}} > \sigma^2_{\text{fleshy}}$). Finally, we expect that the climatic niches of fleshy fruits will be more conserved through time ($\alpha_{\text{dry}} < \alpha_{\text{fleshy}}$). We apply several *hOUwie* models to test these hypotheses and compare our results to those discussed in Vasconcelos et al. (2021). We expect that any differences found between this study and Vasconcelos et al. (2021) are because we can explicitly account for the joint probability of the discrete and continuous characters. We focus our attention on Ericaceae specifically because Vasconcelos et al. (2021) found two counter-intuitive results. Namely, they found that the phenotypic optima of dry fruits were more humid than fleshy fruited lineages, and that the rate of climatic evolution was greater in fleshy fruits than dry fruits.

We included 25 *hOUwie* models within our model set: 2 CID, 10 CD, 10 CID+, and 3 HYB. *Gaultheria* is technically a dry-fruited genus within Ericaceae but has a persistent fleshy calyx that attracts frugivores (Stevens et al. 2004). However, since we are interested in the association between dispersal and fruit type, we code this as fleshy fruited within our dataset. Models are evaluated using the sample size corrected Akaike Information Criterion (AICc) and model averaging is conducted when discussing how our results relate to our hypotheses (Burnham and Anderson 2002). Measurement error is included for each model fit as within species variance (the sample-sized weighted average of the individual species variances following Labra et al. (2009) and Vasconcelos et al. (2021)). We evaluate then model averaged parameter estimates of θ, σ^2, and α for fleshy and dry fruited lineages, as they relate to our

hypotheses and compare our results to Vasconcelos et al. (2021). Finally, we conduct a parametric bootstrap of 100 simulated datasets to evaluate the standard error of our model averaged parameter estimates.

Results

Simulation study

For character-independent (CID) models, our heuristic adaptive sampling algorithm, which uses information from the discrete and continuous characters to guess at mappings, consistently produced more probable mappings than using purely discrete mappings for all models examined. On average, adaptive sampling produced mappings which were roughly 38 log likelihood units better than purely discrete sampling when examining joint probabilities. This was driven primarily by the improved continuous probabilities which were on average 38.4 log likelihood units better. In contrast, the discrete probability of each mapping was similar with discrete-only simulations producing maps that were on average 0.39 log likelihood units better (Table 1; Figure S1). For character-dependent models, the difference was negligible (not shown). This is because when the discrete and continuous character are strongly linked, discrete-only mappings will match the continuous character's distribution quite well.

Most character-dependent models (CD) had lower overall deviations from the generating model across all model types. The RMSE was largest for alpha at 1.76 and 1.65 (if variable alpha) and errors were generally higher for more complex models. All other parameters had relatively similar RMSE, ranging from 0.1 for discrete the rate to 0.75 for σ_2^2. The BMV (BM with variable σ), OUV (OU with variable σ), OUA (OU with variable α), and OUM (OU with variable θ) models generally had the lowest errors, but there were some biases present (Table 2).

Most notably, alpha was biased upwards for OUM and OUV models and under variable alpha models (OUA, OUMA, OUVA, OUMVA), the difference between the alpha estimates tended to be larger than the generating parameter difference. The more complex models had larger error variances but showed similar biases as the simple models. Finally, OUBM models showed a significantly downward biased α, suggesting BM like processes (Figure S2).

Table 1. A comparison of the effectiveness of the adaptive sampling procedure and standard discrete only sampling of maps. Regardless of the sampling procedure, all probabilities are calculated in the same way and so any differences in probabilities reflects each procedure's ability to generate appropriate mappings. 50 regime mappings are used to calculate the likelihood of the parameters. A higher log_e likelihood is better (that is, -16.43 is better than -16.48; 10.54 is better than 9.19)For each model type, data are simulated following our methods with $q_{ij} = 0.1, \alpha_1 = 3, \alpha_2 = 1.5, \sigma_1^2 = 0.35, \sigma_2^2 = 1, \theta_1 = 2,$ and $\theta_2 = 0.75$. The generating parameters are used to evaluate probability of each dataset and thus the probabilities represented here are not necessarily the same as those derived from the MLE. Generally, adaptive sampling improves the joint estimate by improving the probability of the continuous character and is most effective for variable θ models. As expected, discrete only sampling produces regime paintings which better reflect the discrete character than adaptive sampling, but the difference is minor.

Model class	Model type	Sampling procedure	Discrete marginal log_e likelihood	Continuous marginal log_e likelihood	Joint log_e likelihood
CID+	BMV	adaptive sampling	-16.48	10.54	**-10.59**
		discrete only	-16.43	9.19	-10.59
	OUA	adaptive sampling	-15.46	44.34	**25.14**
		discrete only	-15.53	43.11	24.96
	OUV	adaptive sampling	-30.89	47.86	**12.17**
		discrete only	-30.14	46.00	12.11
	OUVA	adaptive sampling	-11.88	36.91	**21.14**
		discrete only	-11.17	36.27	21.08
	OUM	adaptive sampling	-11.94	57.57	**39.08**
		discrete only	-11.19	53.56	32.21
	OUMA	adaptive sampling	-9.94	35.01	**17.39**
		discrete only	-9.38	2.19	-20.48
	OUMV	adaptive sampling	-19.96	20.77	**-15.64**
		discrete only	-14.76	-2.92	-25.83
	OUMVA	adaptive sampling	-13.91	25.47	**7.48**
		discrete only	-13.23	26.36	4.48
	OUBM1	adaptive sampling	-14.26	42.20	**24.39**
		discrete only	-14.88	40.89	24.22
	OUBMV	adaptive sampling	-19.17	49.10	**18.84**
		discrete only	-19.01	33.45	7.71

Table 2. The average accuracy of *hOUwie* parameter estimates across several model classes and types as measured by root-mean-square error (RMSE). RMSE is calculated for each model type by taking the square root of the mean squared error (MSE), where MSE is the average squared difference between the MLE and the simulating parameters. Data is generated with $q_{ij} = 0.1, \alpha_1 = 3, \alpha_2 = 1.5, \sigma_1^2 = 0.35, \sigma_2^2 = 1, \theta_1 = 2,$ and $\theta_2 = 0.75$, and for phylogenies with 25, 100, and 250 taxa. Finally, model fits use either 25, 100, or 250 stochastic maps per likelihood iteration. The table shown here calculates RMSE integrating over all phylogenetic tree sizes and number of stochastic maps (n=8217). Dashes indicate a parameter that is not estimated for a given model type. Generally, character independent (CID+) models had higher errors than character dependent (CD) models. The greatest errors occurred when estimating alpha in variable alpha models for both CD and CID+ model classes. Estimates of the optimum and transition rates generally had the lowest errors.

Model class	Model type	RMSE q	RMSE α_1	RMSE α_2	RMSE σ_1^2	RMSE σ_2^2	RMSE θ_1	RMSE θ_2
CD	BMV	0.12	-	-	0.10	0.28	0.22	-
	OUV	0.11	1.27	-	0.15	0.33	0.05	-
	OUA	0.12	1.55	1.63	0.11	-	0.06	-
	OUM	0.13	1.49	-	0.10	-	0.07	0.13
	OUVA	0.09	1.44	1.11	0.14	0.98	0.06	-
	OUMV	0.16	1.82	-	0.16	0.32	0.07	0.17
	OUMA	0.15	2.11	2.48	0.28	-	0.12	0.50
	OUMVA	0.18	1.62	1.12	0.12	1.07	0.76	1.06
	OUBM1	0.1	2.64	-	0.08	-	0.08	-
	OUBMV	0.09	2.29	-	0.13	2.37	0.08	-
CID+	BMV	0.05	-	-	0.27	10.11	0.24	-
	OUV	0.04	1.13	-	0.32	1.83	0.05	-
	OUA	0.05	2.93	1.34	0.33	-	0.07	-
	OUM	0.09	2.53	-	0.15	-	0.44	0.20
	OUVA	0.05	1.26	1.11	0.27	13.44	0.07	-
	OUMV	0.1	2.50	-	0.16	2.12	1.30	0.68
	OUMA	0.05	8.28	1.27	0.23	-	5.88	0.8
	OUMVA	0.07	5.54	1.24	0.20	9.37	8.76	1.35
	OUBM1	0.05	3.33	-	0.32	-	0.14	-
	OUBMV	0.05	3.50	-	0.27	8.79	0.14	-

Character-independent models with rate heterogeneity models generally performed well in terms of parameter estimates, but as expected, due to their inherit uncertainty, CID+ models had larger errors than CD models. The largest error was estimates of σ_2^2 which had an RMSE of 8.5, although the median error value was only 0.03, suggesting that the large RMSE is driven by a long rightward tail of the estimates. Like CD models, α_1 and α_2 consistently showed the

largest RMSE at 3.6 and 1.2. In general, α was underestimated with medians of -0.4 and -1.4 below the simulating values of 3 and 1.5. This means that models for CID+ models tended to be more BM like even under an OU generated data (Figure S2). Increasing the number of taxa examined improved both CD and CID+ performance. The RMSE for α was nearly cut in half between when moving from 25 tips to 250 tips from 5.2 to 2.8 under CID+ models (Table 3). Nonetheless, some parameters continued to be estimated poorly, such as σ_2^2. Interestingly, increasing the number of stochastic maps improved CID+ performance, but did not substantially improve estimation under CD models (Fig. S2c).

Table 3. Average AIC weight as the number of taxa increases for each model class. Gray cells indicate the AIC weight of the generating model class. In general, as the number of taxa increases the average support for the generating model class increases.

Generating model class	nTaxa	AICwt BM1	AICwt OU1	AICwt CD	AICwt CID+
CD	25	0.12	0.22	0.51	0.15
	100	0.06	0.22	0.70	0.02
	250	0.02	0.14	0.82	0.02
CID+	25	0.28	0.35	0.24	0.14
	100	0.21	0.4	0.23	0.15
	250	0.11	0.34	0.32	0.22

Generally, evidence of CD when it was the generating model was consistent across all model types. The lowest support for the OUA and OUBM1 models at an average AICwt of 0.31 and 0.13. For complex models, such as OUMVA, model support for was 0.81 and highest for OUMV at 0.97. CID+ models fared worse in terms of generating consistent support even when they were the generating model. Models which were difficult to estimate under character dependence were difficult to find consistent support for under character independence. The most extreme case was OUA model for which CID+ model was never chosen as the best supported model. However, models which performed well for CD tended to perform well under CID+. For example, OUM models garnered consistent support when with an average AICwt of 0.733

(Table S1; Figure S3). While the best model under AICc need not be the generating model (for example, for a small dataset a simpler model may lose less information than the generating model) given the size of the simulated trees and distinctness of the models we expect the generating model to generally be the best.

For both CD and CID+ models, support improved when increasing the number of tips analyzed. Support for a CD model when CD was the generating model increased from $w_{CD} = 0.5$ to $w_{CD} = 0.67$ to $w_{CD} = 0.79$ for 25, 100, 250 tips and support for a CID+ model when it was the generating model increased from $w_{CID+} = 0.11$ to $w_{CID+} = 0.15$ to $w_{CID+} = 0.22$ (Table 3). Similarly, increasing the number of regime maps generally improved the fit, but not as much as increasing the number of tips. We found that the false evidence of correlation (as measured by the average AICwt of a character-dependent model when character-independence was the generating model) was generally not an issue for variable θ models (OUM*). Variable θ models had average AICwts for false character-dependence ranging from 0.03 to 0.23 and for none of our simulations models was a CD model best supported. Under a simple OUM model, CID+ models helped correct any potential bias with an average AICwt of 0.68. However, false evidence of correlation was an issue for variable $\sigma_i^2$and α_i models. False support for CD as measured by AIC weight ranged from 0.34 to 0.44 when θ was fixed and α_i and/or σ_i^2 varied. Although CID+ models did not garner much support when these models were fit, OU1 and BM1 models served as reasonable null hypotheses in these cases. In general, we found that when CID models were the generating model, evidence of CID was strongest and when CD models were the generating model, evidence of character dependence was strongest. This suggests that the effect of rate heterogeneity causing false correlations is not as pronounced as other comparative methods (Maddison and FitzJohn 2015; Rabosky and Goldberg 2015).

Seed dispersal and climatic evolution

We found evidence of a character-dependent model over either a simple or hidden state character-independent model, suggesting a link between the climatic niche of Ericaceae lineages and their fruit type (Table S2). The best supported models were OUMVA and OUVA with AIC weights of 0.41 and 0.32 respectively. This suggests that there were character dependent differences in phenotypic optima, rates of evolution, and overall phylogenetic signal. To evaluate support for our hypotheses we examined the model averaged parameter estimates (Table 4). The estimated optimum 0.81 $ln(AI)$ ($\pm$ 0.28) for fleshy fruits suggests a more arid environment for their optimal habitat, and the 0.97 $ln(AI)$ ($\pm$ 0.011) of dry fruits corresponds to a more humid environment (Middleton and Thomas 1997), where AI is measured as mean annual precipitation (P) dived by average annual potential evapotranspiration (PET). However, both optima correspond to non-dryland humid environments. Both $\sigma^2$and α interact to create tip variance, so in addition to σ^2, we measured the stationary variance $V = \frac{\sigma^2}{2\alpha}$. As predicted, we found that Ericaceae lineages with dry fruits were more variable in their climatic niche evolution ($\sigma^2_{dry} = 0.011\ ln(AI)^2 MY^{-1}$, $V_{dry} = 0.37\ ln(AI)^2$) compared to fleshy fruits ($\sigma^2_{fleshy} = 0.007\ ln(AI)^2 MY^{-1}$, $V_{fleshy} = 0.15\ ln(AI)^2$). Additionally, the strength of pull of fleshy fruited lineages was greater than dry fruited lineages ($\alpha_{fleshy} = 0.022 MY^{-1} > \alpha_{dry} = 0.014 MY^{-1}$). This corresponds to phylogenetic half-lives of $t_{1/_{2},dry} = 46.4$ MY and $t_{1/_{2},fleshy} = 30.3$ MY which are 38% and 25% of the total tree height respectively. Transitions to fleshy fruit occurred at 0.0015 transitions per million years which is more than 4.3 times faster than transitions to dry fruits (0.0004 transitions per million years). The waiting time $\left(\frac{1}{q}\right)$ of fleshy fruits ($2{,}500\ MY$) was substantially longer than that of dry fruits ($667\ MY$). Given that the total branch length in

the tree is 10,120 MY, we expect that lineages were typically under the fleshy fruit regime and evolving towards a preference for more humid environments. Perhaps for this reason we found that, on average, lineages were in more arid environments than predicted by the model (average difference of 0.19 AI), with some species expected to be in much more humid environments (difference between current AI and optimal AI ranged from -4.4 to 0.85; Figure 7).

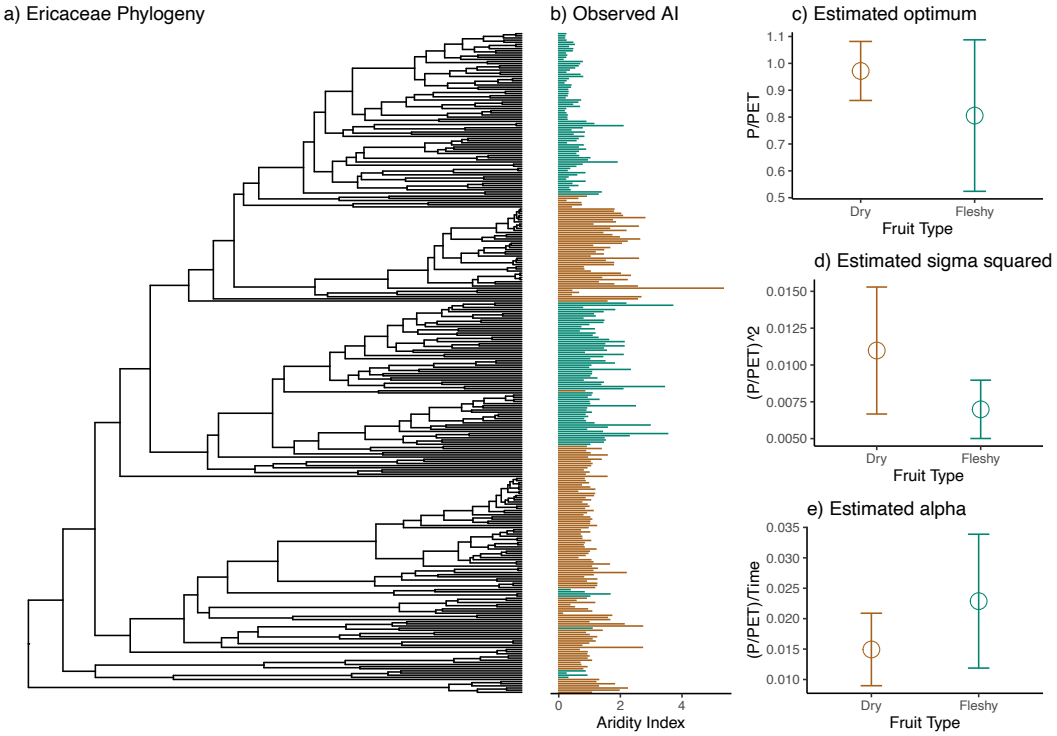

Figure 4. a) Ericaceae phylogeny for which we had data (n=309). b) Ln aridity index dataset where each bar is colored by dry (brown) and fleshy (green) fruit type. c) Model averaged parameter estimates with standard error calculated from 100 parametric bootstraps.

Table 4. Model averaged parameter estimates and standard errors for Ericaceae aridity index and fruit type data. Models with higher AIC weights contribute more overall to the parameter values. The units for α, σ^2, and θ are $\frac{P}{PET} \div time$, $\left(\frac{P}{PET}\right)^2$, and $\frac{P}{PET}$ respectively. P is the average annual precipitation and PET is average annual potential evapotranspiration. Rates of q are measured in transitions per million years.

Continuous parameter estimates				Discrete parameter estimates	
	α	σ^2	θ		
Dry	0.015 (±0.0059)	0.011 (±0.0043)	0.97 (±0.011)	$q_{dry\ to\ fleshy}$	0.0015 (±0.00058)
Fleshy	0.023 (±0.011)	0.007 (±0.002)	0.81 (±0.28)	$q_{fleshy\ to\ dry}$	00036 (±0.000086)

Discussion

Phylogenetic comparative methods have been widely applied to study discrete and continuous characters separately. Due primarily to computational limitations there are few options which jointly evaluate both classes of character. The *hOUwie* framework proposed here overcomes these limitations, and we demonstrate how it is used to test hypotheses of correlated evolution between discrete and continuous characters while accounting for hidden character states and unobserved variation. Our model jointly models discrete and continuous characters by linking both via a common regime painting. However, unlike other similar methods, our likelihood formula explicitly calculates the probability of the underlying regimes. This has the advantage of describing the discrete character evolution probabilistically and allows information from the discrete and continuous characters to jointly contribute to the overall likelihood.

Relationship to existing methods

Considerable progress has been made towards more realistic models of continuous character evolution within the last two decades. Continuous character models which initially relied on either single rate Brownian motion or simple Ornstein-Uhlenbeck models (Felsenstein 1985; Hansen 1997) have seen several extensions to allow for heterogeneity in the evolutionary process as well as the deterministic influence of underlying independent variables. Generally, these models can be classified as either being “hypothesis driven” or “data driven” (Martin et al. 2022). Hypothesis driven models are those which require *a priori* hypotheses regarding where evolutionary rates may differ throughout the phylogeny. These include models which have extended simple single-rate BM to incorporate rate variation based on discrete regime mappings (e.g., O’Meara et al. 2006; Thomas et al. 2006; Revell and Collar 2009; Caetano and Harmon

2017) or more generalized Ornstein-Uhlenbeck models where parameters are allowed to vary based on an underlying regime mapping (e.g., Butler and King 2004; Bartoszek et al. 2012; Beaulieu et al. 2012). In contrast, several methods have focused on the development of data driven, shift-detection methods (which may indeed be used in testing hypotheses, but these hypotheses are not directly used in creating the regime map). These methods utilize an Ornstein-Uhlenbeck process to automatically detect where in the phylogeny evolutionary rates and phenotypic optima shift (Ingram and Mahler 2013b; Uyeda and Harmon 2014; Khabbazian et al. 2016; Bastide et al. 2017). Furthermore, some recently developed methods have allowed for rate variation without the assumption of constant regimes at all. Instead, these models assume the rates themselves evolve and change throughout the phylogeny under various Brownian motion-like processes (Lemey et al. 2010; Eastman et al. 2013; Revell 2021; Martin et al. 2022) or single optima Ornstein-Uhlenbeck processes (Hansen et al. 2008; Mitov et al. 2019). The method presented here is most like the latter group. *hOUwie* attempts to explicitly model the evolution of rate shifts according to regimes which jointly influence discrete and continuous character evolution. The regimes themselves are never fixed a priori and each is evaluated as a partial contribution to the overall probability of the data. The advantage of this approach is that it acknowledges the uncertainty in the underlying regime paintings and allows them to change through time.

Additionally, unlike *hOUwie*, the "hypothesis driven" or "data driven" models do not explicitly account for the joint modeling of the discrete and continuous characters. Most progress in this area has, until recently, been made via phylogenetic logistic regressions (Ives and Garland 2010) or threshold models in which the discrete character is modeled by a continuously varying unobserved lability (Felsenstein 2012; Revell 2014; Cybis et al. 2015). However, these models

rely on more simplistic evolutionary models without character independent rate heterogeneity (such as single rate Brownian motion). This lack of character independent rate heterogeneity has recently been recognized as a potential source of inflated correlation between discrete and continuous characters. Such was the reasoning for the MuSSCRat model (May and Moore 2020). Like *hOUwie*, MuSSCRat allows for character-independent rate heterogeneity following a multiple rate Brownian motion model to be directly contrasted against character correlation to correct for potential biases towards correlation. However, as we describe in detail above, the way the underlying discrete character is calculated in *hOUwie*, as well as how rate heterogeneity is modeled, differs substantially from May and Moore (2020). Finally, Tribble et al. (2021) has recently developed a method which is similar to the one presented here. One of the primary differences between *hOUwie* and the Bayesian pipeline discussed in Tribble et al. (2021) is how discrete character evolution is treated. Specifically, Tribble et al. (2021) assumed that character-independent mappings are generated under the same parameters which best fit their focal discrete character. In contrast, *hOUwie* allows the free estimation of character-independent discrete rates which best fit both discrete and continuous data. This difference may lead to biases against null models in the Tribble et al. (2021) approach since the character-independent regimes are forced to follow a character-dependent discrete model.

Character-independent models and null hypotheses

There is a growing appreciation that comparing constant-rate null models to variable-rate alternative models will consistently favor rate heterogeneity, regardless of whether there is a genuine association with a focal variable (Maddison and FitzJohn 2015; Rabosky and Goldberg 2015; Beaulieu and O'Meara 2016; Uyeda et al. 2018; O'Meara and Beaulieu 2021; Boyko and

505 Beaulieu 2022). This problem, termed the “straw-man effect” by May and Moore (2020), has
506 been demonstrated to lead to nearly 100% error rates for evidence of discrete character
507 correlation (Maddison and FitzJohn 2015; Boyko and Beaulieu 2022), and has severely biased
508 evidence towards state-dependent speciation and extinction (Rabosky and Goldberg 2015;
509 Beaulieu and O’Meara 2016). Given these often-overwhelming error rates in other comparative
510 methods, we expected to find a similarly consistent bias towards correlation between discrete and
511 continuous characters. However, we found that support for single rate character-independent null
512 models was greater than character-dependent models even when simulated under character-
513 independent models with rate heterogeneity. Although the inclusion of explicit multi-rate
514 character independent models (CID+) models did help reduce evidence of false correlation in
515 some cases, by and large, simplistic null models performed admirably. This is not to say that the
516 error rates for discrete and continuous character correlation should be dismissed outright. If our
517 simulations correctly assess that nearly one-third of results find false evidence of a correlation
518 between continuous character rates of evolution and discrete characters, then better null models
519 are certainly needed. But, in comparison to the profound effect that model misspecification has
520 had in other comparative analyses (Beaulieu and O’Meara 2016; Boyko and Beaulieu 2022), the
521 joint models tested here have substantially lower error rates.
522 We suspect that part of the reason that the correlation between discrete and continuous
523 characters is less susceptible to “straw-man” effects than other PCMs is related to the
524 inefficiency of sampling potential maps from the univariate stochastic mapping model. A
525 common approach to fitting OU models involves simulating many stochastic maps to represent
526 underlying regimes from parameters estimated only from the discrete character (Revell 2013).
527 The resulting distribution of underlying regimes will therefore reflect a distribution appropriate

for the discrete character, but not necessarily suitable for the continuous character. This is especially true if the continuous character is unlinked to the focal discrete character. Indeed, we found that if the discrete and continuous characters are unlinked, most stochastic maps, even though good descriptions of the discrete characters, were completely inadequate representations of continuous regimes. Thus, any joint model with these maps contributed little to the overall likelihood. Under our simulation protocol, for a typical run, 90% of the total likelihood for the best set of parameters came from just 2% of the attempted maps.

In some ways the substantial contributions of only a few underlying regimes to the overall likelihood is good. First, it makes spurious links between a randomly distributed discrete character and a continuous character more unlikely since associations between regimes and continuous variables tend to be specific. This ultimately reduces the potential "straw-man" effect. Second, the continuous characters can inform the placement of shared regimes and therefore shift detection methods, where the continuous data are all that provides information about regimes shifts (Ingram and Mahler 2013; Uyeda and Harmon 2014; Khabbazian et al. 2016; Bastide et al. 2017), may be appropriate across a broad range of scenarios. However, this property also makes sampling a good set of regimes to get an accurate estimate of the likelihood difficult and is why the development of our adaptive sampling heuristics was necessary. Adaptive sampling, in combination with our approximation of the joint conditional distributions, helped make parameter estimation more accurate. Increasing the amount of sampled regime mappings is useful in improving precision (Fig 5c), at the cost of longer run time.

Interplay of continuous, discrete, and hidden traits

In many studies that deal with the correlation of discrete and continuous traits, it is often assumed that the discrete trait functions as the independent trait and the continuous trait as the dependent trait. This assumption is baked into methods that map the discrete trait first and then analyze the continuous trait given these mappings, but it would be easy to fall into this form of thinking even with *hOUwie*, which does not have this assumption. Instead, *hOUwie* can help understand whether and how traits are correlated. For example, one could see if mammal body size correlates with trophic level: are hypercarnivores larger on average than herbivores? It could be that an herbivorous (discrete character) beaver evolves a taste for meat and then grows bigger (continuous character) so it can take down bigger prey; it could be that once things get to be the size of a bison (continuous character) they start adding more and more rodents to their diet, eventually becoming carnivores (discrete character). Causality can go both directions, and of course both traits may be evolving based on some other third trait and not functionally related to each other.

hOUwie is part of a series of hidden state models developed by our research groups (i.e., Beaulieu et al. 2013; Beaulieu and O'Meara 2016; Caetano et al. 2018; Boyko and Beaulieu 2021, 2022; Vasconcelos et al. 2022). One misconception we have noted in use of these methods is the thought that there is a single, discrete, hidden character in the biology. These models do model a single hidden character (with potentially many states), but this could be reflecting multiple characters evolving together or other factors that change in a heritable manner through time. It is a way to allow heterogeneity, especially by factors that vary by clades. With *hOUwie*, this heterogeneity can affect the discrete trait, the continuous trait, both, or neither.

575 Here we revaluated three hypotheses related to climatic niche evolution and seed
576 dispersal and found that: (1) the climatic optima of dry fruits was more humid than fleshy fruits
577 ($\theta_{fleshy} < \theta_{dry}$), (2) lineages with dry fruits had faster rates of climatic niche evolution ($\sigma^2_{dry} >$
578 σ^2_{fleshy}), and (3) climatic niches of fleshy fruits are more conserved through time ($\alpha_{dry} <$
579 α_{fleshy}). In contrast to previous findings, the higher rate and stationary variance of climatic niche
580 evolution for dry seeds matched our original hypothesis (Vasconcelos et al. 2021). This is to be
581 expected because abiotically dispersed seeds are likely to be more erratic in their dispersal
582 patterns (Schupp 1993; Westoby et al. 1996). Additionally, that our results differ from previous
583 findings (Vasconcelos et al. 2021) suggests that jointly modeling climatic niche evolution
584 alongside fruit type changed our parameter estimation in a meaningful way.

585 Our final hypothesis, which stated that fleshy, biotically dispersed, seeds are more likely
586 to be associated with humid environments, was not supported. However, it has been suggested
587 that a trade-off between seed persistence, seed size, and dispersal strategies can be also common
588 in arid environments (Venable and Brown 1988; Nunes et al. 2017). Specifically, large seed size
589 may occasionally help withstand unfavorable conditions associated with increased aridity (Nunes
590 et al. 2017). With an increased seed size, biotic seed dispersal and fleshy fruits, may become
591 necessary for seed dispersal. This may be the case for Styphelieae, which is distributed in the
592 arid Australian heathland and, of all predominately fleshy-fruited groups, lies the furthest from
593 the inferred aridity optima. Additionally, it has been found that the proportion of abiotically
594 dispersed seeds increases as elevation increases, due to the decreasing availability of frugivores
595 (Chapman et al. 2016). Given that several radiations of Ericaceae lineages are associated with
596 montane habitats (Schwery et al. 2015), it may be that the distribution of dry and fleshy fruits are

a consequence of elevation rather than being directly linked to climatic niche evolution. Finally, it has been noted Ericaceae lineages are often found in well-leached soils and epiphytic habitats (Schwery et al. 2015). If associations with soil type are more important than links to climatic optima, we may expect that fruit-dependent climatic optima are consequence of unmodeled factors. Although our modeling explicitly considers hidden variables that may lead to rate heterogeny, if the proposed hidden variable (soil condition) is closely linked to our modeled variable (aridity), then we may not be able to detect the presence of hidden variation. This may be the case between soil condition and aridity (Moreno-Jiménez et al. 2019).

Caveats and possible extensions

There are three important caveats to our proposed modeling framework. First, our discrete mapping probability, $P(D, z|\vartheta, \psi)$, is only an approximation. What we calculate is the probability of starting in a particular state i and ending a particular state j, summed over all possible paths. However, the continuous model probability is based off a particular pathway history that is defined throughout the entire branch (Hansen 1997). Ultimately, this means that the underlying regimes are not treated identically for the continuous and discrete characters. The second caveat is that we do not force *hOUwie* to sum over all possible mappings z. This is because the number of mappings will grow exponentially as the number of nodes and internodes increases and the computation will quickly become infeasible (see Jones et al. 2020). Although this may not be entirely necessary since we have shown that only a small percentage of possible mappings contribute to the overall joint probability. Nonetheless, an ideal solution could be the use Markov-Modulated Ornstein-Uhlenbeck models (Huang et al. 2016) since this would remove the need for a regime mapping approach, but these have yet to be applied in phylogenetic

comparative biology. *hOUwie* currently only deals with one discrete and one continuous trait at a time – a set of discrete traits can be handled by converting them to a single multistate character, but incorporating multiple continuous traits requires adding correlations between them. Finally, it is possible to extend *hOUwie* to include state-dependent speciation and extinction dynamics which have been shown to influence the distribution of discrete characters (Maddison 2006) and would therefore influence continuous characters if the two were linked. However, this extension would require a different calculation of the underlying regime mapping probability. Approaches for stochastically mapping SSE models already exist (Freyman and Höhna 2019), so the largest remaining challenge of this extension would be generating high joint probability mappings.

Concluding remarks

The use of pre-defined discrete character mappings can be useful for testing hypotheses which rely on distinct, well-defined differences in the evolutionary histories of lineages. However, this approach assumes that the underlying mapping is known with complete accuracy and ignores the probabilistic nature of discrete regimes. *hOUwie*'s methodology integrates over the uncertainty of high probability character mappings and relies on the interpretation of parameter estimates from contrasting model structures to find evidence for hypotheses. Rather than assuming an *a priori* mapping, *hOUwie* can utilize the mutual information about the discrete and continuous characters to learn something about the underlying regimes evolution.

Tables

Table 1. A comparison of the effectiveness of the adaptive sampling procedure and standard discrete only sampling of maps. Regardless of the sampling procedure, all probabilities are calculated in the same way and so any differences in probabilities reflects each procedure's ability to generate appropriate mappings. 50 regime mappings are used to calculate the likelihood of the parameters. A higher log_e likelihood is better (that is, -16.43 is better than -16.48; 10.54 is better than 9.19)For each model type, data are simulated following our methods with $q_{ij} = 0.1, \alpha_1 = 3, \alpha_2 = 1.5, \sigma_1^2 = 0.35, \sigma_2^2 = 1, \theta_1 = 2,$ and $\theta_2 = 0.75$. The generating parameters are used to evaluate probability of each dataset and thus the probabilities represented here are not necessarily the same as those derived from the MLE. Generally, adaptive sampling improves the joint estimate by improving the probability of the continuous character and is most effective for variable θ models. As expected, discrete only sampling produces regime paintings which better reflect the discrete character than adaptive sampling, but the difference is minor.

Model class	Model type	Sampling procedure	Discrete marginal log_e likelihood	Continuous marginal log_e likelihood	Joint log_e likelihood
CID+	BMV	adaptive sampling	-16.48	10.54	**-10.59**
		discrete only	-16.43	9.19	-10.59
	OUA	adaptive sampling	-15.46	44.34	**25.14**
		discrete only	-15.53	43.11	24.96
	OUV	adaptive sampling	-30.89	47.86	**12.17**
		discrete only	-30.14	46.00	12.11
	OUVA	adaptive sampling	-11.88	36.91	**21.14**
		discrete only	-11.17	36.27	21.08
	OUM	adaptive sampling	-11.94	57.57	**39.08**
		discrete only	-11.19	53.56	32.21
	OUMA	adaptive sampling	-9.94	35.01	**17.39**
		discrete only	-9.38	2.19	-20.48
	OUMV	adaptive sampling	-19.96	20.77	**-15.64**
		discrete only	-14.76	-2.92	-25.83
	OUMVA	adaptive sampling	-13.91	25.47	**7.48**
		discrete only	-13.23	26.36	4.48
	OUBM1	adaptive sampling	-14.26	42.20	**24.39**
		discrete only	-14.88	40.89	24.22
	OUBMV	adaptive sampling	-19.17	49.10	**18.84**
		discrete only	-19.01	33.45	7.71

Table 2. The average accuracy of *hOUwie* parameter estimates across several model classes and types as measured by root-mean-square error (RMSE). RMSE is calculated for each model type by taking the square root of the mean squared error (MSE), where MSE is the average squared difference between the MLE and the simulating parameters. Data is generated with $q_{ij} = 0.1, \alpha_1 = 3, \alpha_2 = 1.5, \sigma_1^2 = 0.35, \sigma_2^2 = 1, \theta_1 = 2,$ and $\theta_2 = 0.75$, and for phylogenies with 25, 100, and 250 taxa. Finally, model fits use either 25, 100, or 250 stochastic maps per likelihood iteration. The table shown here calculates RMSE integrating over all phylogenetic tree sizes and number of stochastic maps (n=8217). Dashes indicate a parameter that is not estimated for a given model type. Generally, character independent (CID+) models had higher errors than character dependent (CD) models. The greatest errors occurred when estimating alpha in variable alpha models for both CD and CID+ model classes. Estimates of the optimum and transition rates generally had the lowest errors.

Model class	Model type	RMSE q	RMSE α_1	RMSE α_2	RMSE σ_1^2	RMSE σ_2^2	RMSE θ_1	RMSE θ_2
CD	BMV	0.12	-	-	0.10	0.28	0.22	-
	OUV	0.11	1.27	-	0.15	0.33	0.05	-
	OUA	0.12	1.55	1.63	0.11	-	0.06	-
	OUM	0.13	1.49	-	0.10	-	0.07	0.13
	OUVA	0.09	1.44	1.11	0.14	0.98	0.06	-
	OUMV	0.16	1.82	-	0.16	0.32	0.07	0.17
	OUMA	0.15	2.11	2.48	0.28	-	0.12	0.50
	OUMVA	0.18	1.62	1.12	0.12	1.07	0.76	1.06
	OUBM1	0.1	2.64	-	0.08	-	0.08	-
	OUBMV	0.09	2.29	-	0.13	2.37	0.08	-
CID+	BMV	0.05	-	-	0.27	10.11	0.24	-
	OUV	0.04	1.13	-	0.32	1.83	0.05	-
	OUA	0.05	2.93	1.34	0.33	-	0.07	-
	OUM	0.09	2.53	-	0.15	-	0.44	0.20
	OUVA	0.05	1.26	1.11	0.27	13.44	0.07	-
	OUMV	0.1	2.50	-	0.16	2.12	1.30	0.68
	OUMA	0.05	8.28	1.27	0.23	-	5.88	0.8
	OUMVA	0.07	5.54	1.24	0.20	9.37	8.76	1.35
	OUBM1	0.05	3.33	-	0.32	-	0.14	-
	OUBMV	0.05	3.50	-	0.27	8.79	0.14	-

Table 3. Average AIC weight as the number of taxa increases for each model class. Gray cells indicate the AIC weight of the generating model class. In general, as the number of taxa increases the average support for the generating model class increases.

Generating model class	nTaxa	AICwt BM1	AICwt OU1	AICwt CD	AICwt CID+
CD	25	0.12	0.22	0.51	0.15
	100	0.06	0.22	0.70	0.02
	250	0.02	0.14	0.82	0.02
CID+	25	0.28	0.35	0.24	0.14
	100	0.21	0.4	0.23	0.15
	250	0.11	0.34	0.32	0.22

Table 4. Model averaged parameter estimates and standard errors for Ericaceae aridity index and fruit type data. Models with higher AIC weights contribute more overall to the parameter values. The units for α, σ^2, and θ are $\frac{P}{PET} \div time$, $\left(\frac{P}{PET}\right)^2$, and $\frac{P}{PET}$ respectively. P is the average annual precipitation and PET is average annual potential evapotranspiration. Rates of q are measured in transitions per million years.

Continuous parameter estimates				Discrete parameter estimates	
	α	σ^2	θ		
Dry	0.015 (±0.0059)	0.011 (±0.0043)	0.97 (±0.011)	$q_{dry\ to\ fleshy}$	0.0015 (±0.00058)
Fleshy	0.023 (±0.011)	0.007 (±0.002)	0.81 (±0.28)	$q_{fleshy\ to\ dry}$	00036 (±0.000086)

Figures

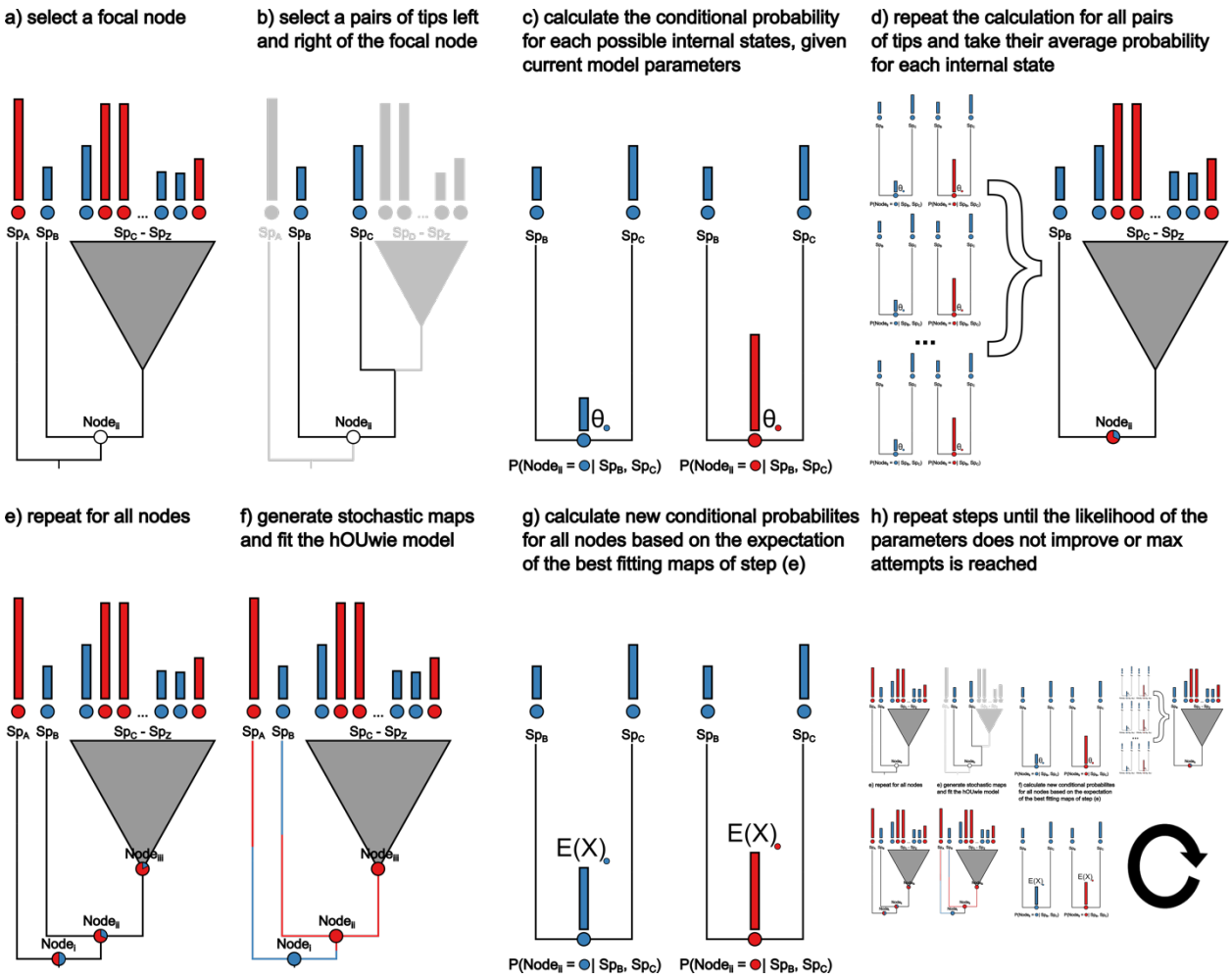

Figure 1. A visual representation of the algorithm underlying the calculation of conditional node probabilities and the adaptive sampling procedure. The goal of the procedure is to produce underlying regime paintings well suited to both the discrete and continuous character. a) select the focal node for which we will be calculating the joint conditional probabilities of the discrete and continuous characters. b) on each side of the node we select a pair of tips. c) the conditional probability of the observed discrete and continuous character is calculated for each discrete regime state with an ancestral continuous value equal to θ of that regime state. d) the conditional probability of the focal node is calculated as the average probability of each regime state for all pairs of observed tips. e) the conditional probabilities are calculated for all internal nodes. This can be turned off within *hOUwie* by setting the sample_nodes argument to false. f) A stochastic map is generating using forward simulation rejection sampling. g) adaptive sampling uses the highest joint probability of previously generated underling regimes to generate a set of ancestral continuous character values. This differs from previous ancestral values because instead of assuming the value θ for each regime state, it calculates the expected value given the root state and regime mapping for that particular node. h) we repeat steps d) through g) until the joint likelihood of the set of underlying regimes does not improve.

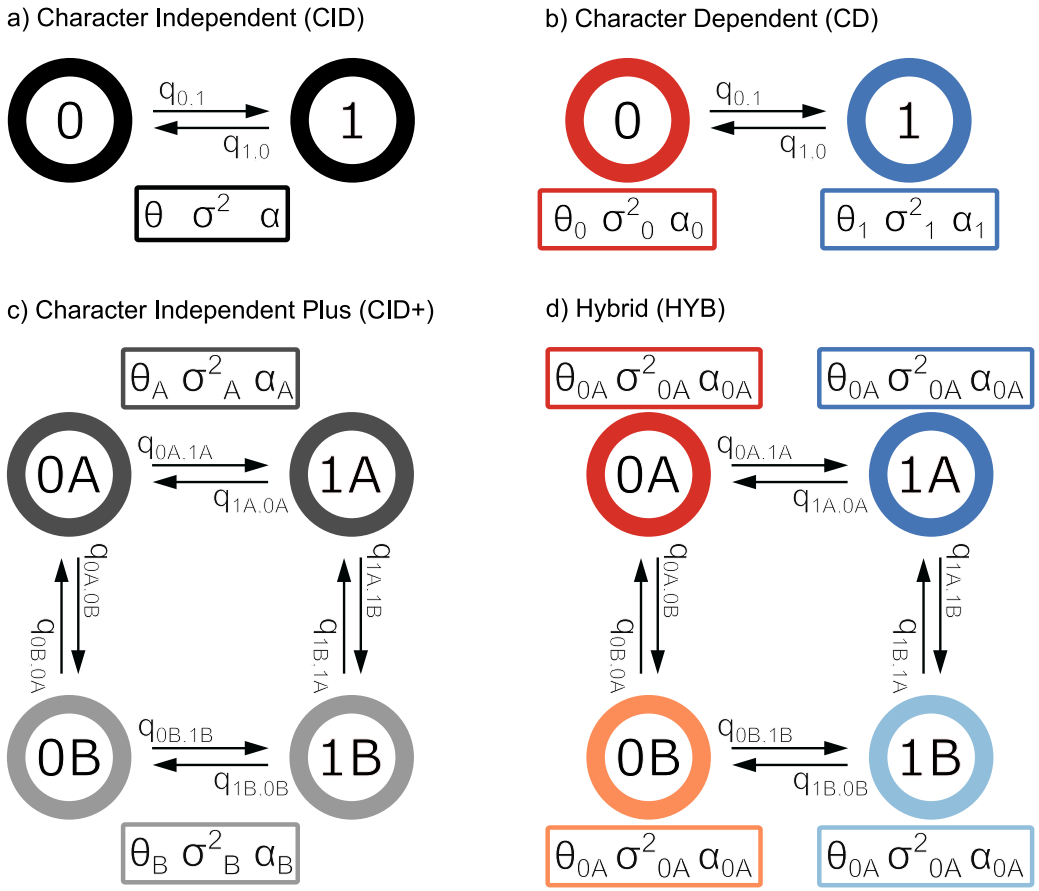

Figure 2. A state-transition diagram describing the model classes allowable in hOUwie. Each panel is comprised of observed discrete states 0 and 1 with possible hidden states A and B. Transitions between states are described with the q parameter. Continuous model parameters appear in a box below the states they describe, and their association is displayed with a subscript specific to that state. a) A simple character independent model in which the two observed states do not influence the continuous character which will have the same θ, σ^2, α throughout the phylogeny. b) A character dependent model in which the continuous character depends on the discrete character by virtue of θ, σ^2, α being associated with a particular observed discrete state. c) A character independent model with rate heterogeneity. The two observed states (0 and 1) are not directly linked to the continuous character. However, the continuous character is still allowed to have multiple θ, σ^2, α describing its evolution, but these parameters are associated with hidden states A and B. d) A hybrid model in which each combined observed and hidden state is allowed to have its own θ, σ^2, α. Under this model, the continuous character is linked to both character dependent differences (parameters associated with 0 and 1) and character independent differences (A and B). Though this diagram shows a binary observed and hidden character, either can have more states (up to 26 states for each in theory, though few datasets will have enough power to estimate the necessary number of parameters).

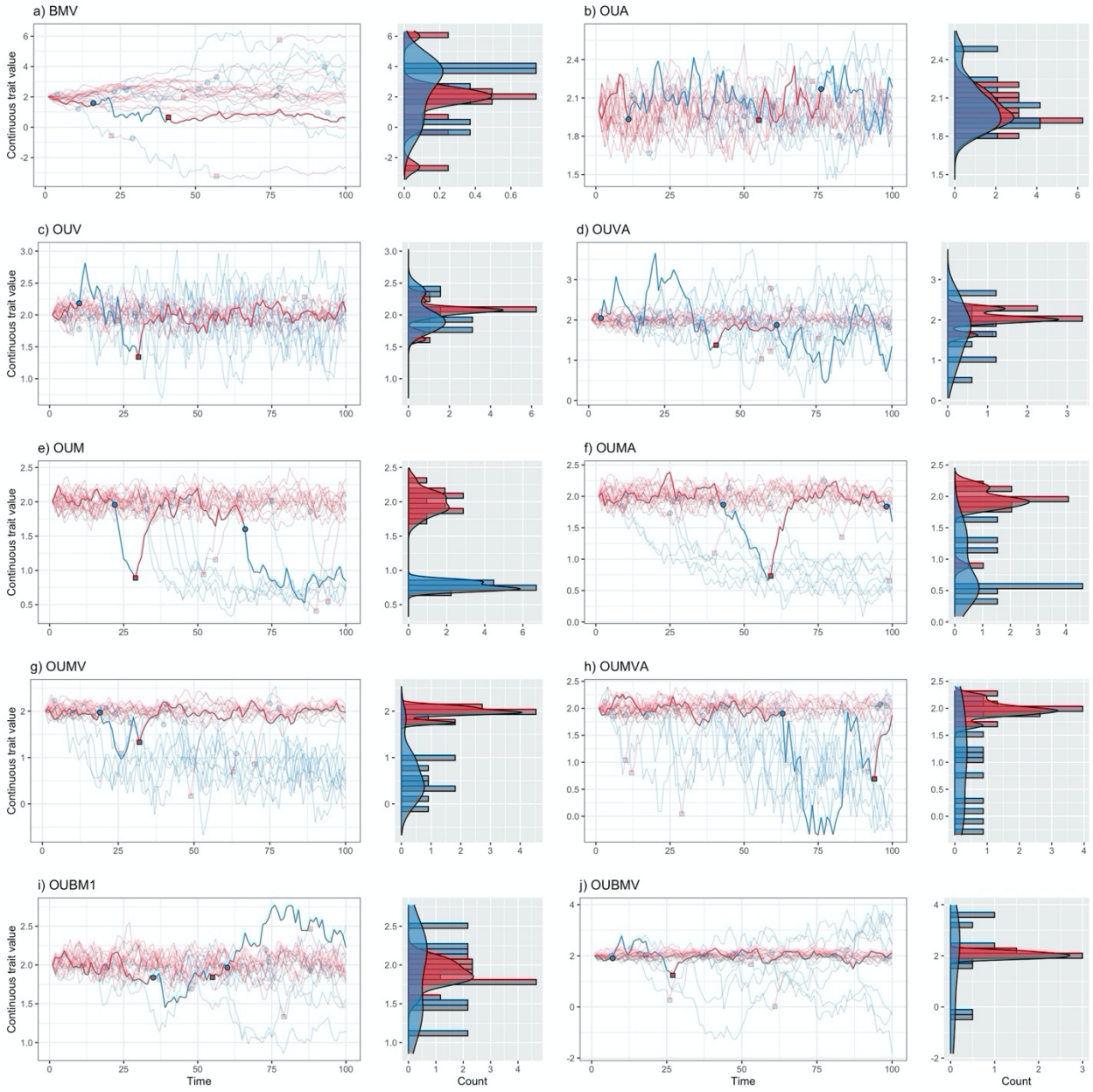

Figure 3. A visual representation of binary discrete character *hOUwie* model types. Discrete time forward simulations are conducted starting in the red state and the distribution of the continuous character is plotted on the right as a histogram and density plot. Each line represents a continuous character value at some time. Transitions occur at colored points and each line is colored by the current discrete state. 100 time-steps are simulated with the same parameters as our simulation study ($q_{ij} = 0.1, \alpha_1 = 3, \alpha_2 = 1.5, \sigma_1^2 = 0.35, \sigma_2^2 = 1, \theta_1 = 2,$ and $\theta_2 = 0.75$). The highlighted line was randomly chosen from the set in which at least one discrete state transition occurred.

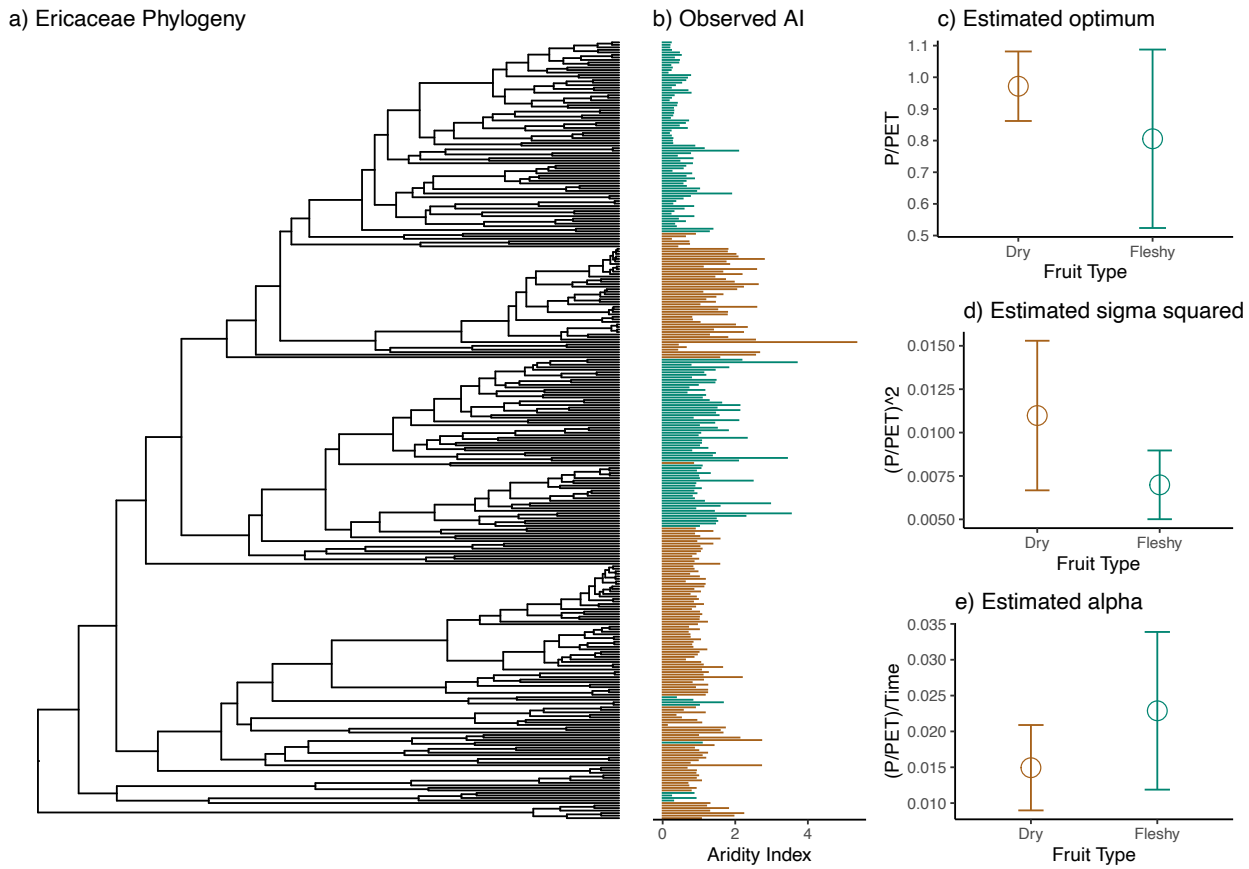

732

733 **Figure 4.** a) Ericaceae phylogeny for which we had data (n=309). b) Ln aridity index dataset
734 where each bar is colored by dry (brown) and fleshy (green) fruit type. c) Model averaged
735 parameter estimates with standard error calculated from 100 parametric bootstraps.
736

Literature cited

Bartoszek K., Pienaar J., Mostad P., Andersson S., Hansen T.F. 2012. A phylogenetic comparative method for studying multivariate adaptation. Journal of Theoretical Biology. 314:204–215.

Bastide P., Mariadassou M., Robin S. 2017. Detection of adaptive shifts on phylogenies by using shifted stochastic processes on a tree. Journal of the Royal Statistical Society: Series B (Statistical Methodology). 79:1067–1093.

Beaulieu J.M., Jhwueng D.-C., Boettiger C., O'Meara B.C. 2012. Modeling Stabilizing Selection: Expanding the Ornstein–Uhlenbeck Model of Adaptive Evolution. Evolution. 66:2369–2383.

Beaulieu J.M., O'Meara B.C. 2016. Detecting Hidden Diversification Shifts in Models of Trait-Dependent Speciation and Extinction. Syst Biol. 65:583–601.

Beaulieu J.M., O'Meara B.C., Donoghue M.J. 2013. Identifying Hidden Rate Changes in the Evolution of a Binary Morphological Character: The Evolution of Plant Habit in Campanulid Angiosperms. Syst Biol. 62:725–737.

Boyko, J., & Beaulieu, J. M. (2022, April 1). Reducing the biases in false correlations between discrete characters. https://doi.org/10.32942/osf.io/e2kj8

Boyko J.D., Beaulieu J.M. 2021. Generalized hidden Markov models for phylogenetic comparative datasets. Methods Ecol Evol. 12:468–478.

Burnham K.P., Anderson D.R. 2002. Model selection and multimodel inference: a practical information-theoretic approach. New York: Springer.

Butler M.A., King A.A. 2004. Phylogenetic Comparative Analysis: A Modeling Approach for Adaptive Evolution. The American Naturalist. 164:683–695.

Caetano D.S., Harmon L.J. 2017. ratematrix: An R package for studying evolutionary integration among several traits on phylogenetic trees. Methods in Ecology and Evolution. 8:1920–1927.

Caetano D.S., O'Meara B.C., Beaulieu J.M. 2018. Hidden state models improve state-dependent diversification approaches, including biogeographical models: HMM and the adequacy of SSE models. Evolution. 72:2308–2324.

Chapman H., Cordeiro N.J., Dutton P., Wenny D., Kitamura S., Kaplin B., Melo F.P.L., Lawes M.J. 2016. Seed-dispersal ecology of tropical montane forests. Journal of Tropical Ecology. 32:437–454.

Cressler C.E., Butler M.A., King A.A. 2015. Detecting Adaptive Evolution in Phylogenetic Comparative Analysis Using the Ornstein–Uhlenbeck Model. Systematic Biology. 64:953–968.

772 Cybis G.B., Sinsheimer J.S., Bedford T., Mather A.E., Lemey P., Suchard M.A. 2015.
773 ASSESSING PHENOTYPIC CORRELATION THROUGH THE MULTIVARIATE
774 PHYLOGENETIC LATENT LIABILITY MODEL. Ann Appl Stat. 9:969–991.

775 Eastman J.M., Wegmann D., Leuenberger C., Harmon L.J. 2013. Simpsonian "Evolution by
776 Jumps" in an Adaptive Radiation of Anolis Lizards. arXiv:1305.4216 [q-bio].

777 Felsenstein J. 1985. Phylogenies and the Comparative Method. Am. Nat. 125:1–15.

778 Felsenstein J. 2004. Inferring phylogenies. Sinauer associates Sunderland, MA.

779 Felsenstein J. 2012. A Comparative Method for Both Discrete and Continuous Characters Using
780 the Threshold Model. The American Naturalist. 179:145–156.

781 Foster S., Janson C.H. 1985. The relationship between seed size and establishment conditions in
782 tropical woody plants. Ecology. 66:773–780.

783 Freyman W.A., Höhna S. 2019. Stochastic Character Mapping of State-Dependent
784 Diversification Reveals the Tempo of Evolutionary Decline in Self-Compatible
785 Onagraceae Lineages. Systematic Biology. 68:505–519.

786 Hansen T.F. 1997. Stabilizing Selection and the Comparative Analysis of Adaptation. Evolution.
787 51:1341–1351.

788 Hansen T.F. 2014. Use and Misuse of Comparative Methods in the Study of Adaptation. In:
789 Garamszegi L.Z., editor. Modern Phylogenetic Comparative Methods and Their
790 Application in Evolutionary Biology. Berlin, Heidelberg: Springer Berlin Heidelberg. p.
791 351–379.

792 Hansen T.F., Pienaar J., Orzack S.H. 2008. A Comparative Method for Studying Adaptation to a
793 Randomly Evolving Environment. Evolution. 62:1965–1977.

794 Ho L. si, Ané C. 2014a. A Linear-Time Algorithm for Gaussian and Non-Gaussian Trait
795 Evolution Models. Syst Biol. 63:397–408.

796 Ho L.S.T., Ané C. 2014b. Intrinsic inference difficulties for trait evolution with Ornstein-
797 Uhlenbeck models. Methods in Ecology and Evolution. 5:1133–1146.

798 Howe H.F., Smallwood J. 1982. Ecology of Seed Dispersal. Annual Review of Ecology and
799 Systematics. 13:201–228.

800 Huang G., Jansen H.M., Mandjes M., Spreij P., Turck K.D. 2016. Markov-modulated Ornstein-
801 Uhlenbeck processes. Advances in Applied Probability. 48:235–254.

802 Ingram T., Mahler D.L. 2013a. SURFACE: detecting convergent evolution from comparative
803 data by fitting Ornstein-Uhlenbeck models with stepwise Akaike Information Criterion.
804 Methods in ecology and evolution. 4:416–425.

Ingram T., Mahler D.L. 2013b. SURFACE: detecting convergent evolution from comparative data by fitting Ornstein-Uhlenbeck models with stepwise Akaike Information Criterion. Methods in Ecology and Evolution. 4:416–425.

Ives A.R., Garland T. 2010. Phylogenetic Logistic Regression for Binary Dependent Variables. Syst Biol. 59:9–26.

Jones C.T., Youssef N., Susko E., Bielawski J.P. 2020. A Phenotype–Genotype Codon Model for Detecting Adaptive Evolution. Systematic Biology. 69:722–738.

Khabbazian M., Kriebel R., Rohe K., Ané C. 2016. Fast and accurate detection of evolutionary shifts in Ornstein–Uhlenbeck models. Methods in Ecology and Evolution. 7:811–824.

Labra A., Pienaar J., Hansen T.F. 2009. Evolution of Thermal Physiology in Liolaemus Lizards: Adaptation, Phylogenetic Inertia, and Niche Tracking. The American Naturalist. 174:204–220.

Lemey P., Rambaut A., Welch J.J., Suchard M.A. 2010. Phylogeography Takes a Relaxed Random Walk in Continuous Space and Time. Molecular Biology and Evolution. 27:1877–1885.

Levin S.A., Muller-Landau *Helene C., Nathan *Ran, Chave *Jérôme. 2003. The Ecology and Evolution of Seed Dispersal: A Theoretical Perspective. Annual Review of Ecology, Evolution, and Systematics. 34:575–604.

Lorts C.M., Briggeman T., Sang T. 2008. Evolution of fruit types and seed dispersal:A phylogenetic and ecological snapshot. Journal of Systematics and Evolution. 46:396.

Maddison W.P. 2006. Confounding Asymmetries in Evolutionary Diversification and Character Change. Evolution. 60:1743–1746.

Maddison W.P., FitzJohn R.G. 2015. The Unsolved Challenge to Phylogenetic Correlation Tests for Categorical Characters. Syst Biol. 64:127–136.

Maddison W.P., Midford P.E., Otto S.P., Oakley T. 2007. Estimating a Binary Character's Effect on Speciation and Extinction. Syst Biol. 56:701–710.

Mahler D.L., Ingram T., Revell L.J., Losos J.B. 2013. Exceptional convergence on the macroevolutionary landscape in island lizard radiations. Science. 341:292–295.

Martin B.S., Bradburd G.S., Harmon L.J., Weber M.G. 2022. Modeling the Evolution of Rates of Continuous Trait Evolution. :2022.03.18.484930.

May M.R., Moore B.R. 2020. A Bayesian Approach for Inferring the Impact of a Discrete Character on Rates of Continuous-Character Evolution in the Presence of Background-Rate Variation. Syst Biol. 69:530–544.

Middleton N., Thomas D. 1997. World atlas of desertification.. ed. 2. .

Mitov V., Bartoszek K., Stadler T. 2019. Automatic generation of evolutionary hypotheses using mixed Gaussian phylogenetic models. Proceedings of the National Academy of Sciences. 116:16921–16926.

Moreno-Jiménez E., Plaza C., Saiz H., Manzano R., Flagmeier M., Maestre F.T. 2019. Aridity and reduced soil micronutrient availability in global drylands. Nat Sustain. 2:371–377.

Nielsen R. 2002. Mapping Mutations on Phylogenies. Systematic Biology. 51:729–739.

Nunes A., Köbel M., Pinho P., Matos P., Bello F. de, Correia O., Branquinho C. 2017. Which plant traits respond to aridity? A critical step to assess functional diversity in Mediterranean drylands. Agricultural and Forest Meteorology. 239:176–184.

O'Meara B. 2008. Using Trees: Myrmecocystus Phylogeny and Character Evolution and New Methods for Investigating Trait Evolution and Species Delimitation (PhD Dissertation). Nat Prec.:1–1.

O' Meara, B., & Beaulieu, J. M. (2021, November 6). Potential survival of some, but not all, diversification methods. https://doi.org/10.32942/osf.io/w5nvd

O'Meara B.C., Ané C., Sanderson M.J., Wainwright P.C. 2006. Testing for Different Rates of Continuous Trait Evolution Using Likelihood. Evolution. 60:922–933.

Pagel M. 1994. Detecting correlated evolution on phylogenies: a general method for the comparative analysis of discrete characters. Proc. R. Soc. B: Biol. Sci. 255:37–45.

Pupko T., Pe I., Shamir R., Graur D. 2000. A Fast Algorithm for Joint Reconstruction of Ancestral Amino Acid Sequences. Mol Biol Evol. 17:890–896.

Rabosky D.L., Goldberg E.E. 2015. Model Inadequacy and Mistaken Inferences of Trait-Dependent Speciation. Syst Biol. 64:340–355.

Rao, V., & Teh, Y. W. (2013). Fast MCMC Sampling for Markov Jump Processes and Extensions. Journal of Machine Learning Research, 14(11).

Revell L.J. 2013. A Comment on the Use of Stochastic Character Maps to Estimate Evolutionary Rate Variation in a Continuously Valued Trait. Systematic Biology. 62:339–345.

Revell L.J. 2014. Ancestral Character Estimation Under the Threshold Model from Quantitative Genetics. Evolution. 68:743–759.

Revell L.J. 2021. A variable-rate quantitative trait evolution model using penalized-likelihood. PeerJ. 9:e11997.

Revell L.J., Collar D.C. 2009. Phylogenetic Analysis of the Evolutionary Correlation Using Likelihood. Evolution. 63:1090–1100.

871 Schupp E.W. 1993. Quantity, quality and the effectiveness of seed dispersal by animals.
872 Vegetatio. 107:15–29.

873 Schwery O., Onstein R.E., Bouchenak-Khelladi Y., Xing Y., Carter R.J., Linder H.P. 2015. As
874 old as the mountains: the radiations of the Ericaceae. New Phytologist. 207:355–367.

875 Steel M., Penny D. 2000. Parsimony, Likelihood, and the Role of Models in Molecular
876 Phylogenetics. Mol Biol Evol. 17:839–850.

877 Stevens P.F., Luteyn J., Oliver E.G.H., Bell T.L., Brown E.A., Crowden R.K., George A.S.,
878 Jordan G.J., Ladd P., Lemson K., Mclean C.B., Menadue Y., Pate J.S., Stace H.M.,
879 Weiller C.M. 2004. Ericaceae. In: Kubitzki K., editor. Flowering Plants · Dicotyledons:
880 Celastrales, Oxalidales, Rosales, Cornales, Ericales. Berlin, Heidelberg: Springer. p. 145–
881 194.

882 Thomas G.H., Freckleton R.P., Székely T. 2006. Comparative analyses of the influence of
883 developmental mode on phenotypic diversification rates in shorebirds. Proceedings of the
884 Royal Society B: Biological Sciences. 273:1619–1624.

885 Toljagić O., Voje K.L., Matschiner M., Liow L.H., Hansen T.F. 2018. Millions of Years Behind:
886 Slow Adaptation of Ruminants to Grasslands. Syst Biol. 67:145–157.

887 Tribble C.M., May M.R., Jackson-Gain A., Zenil-Ferguson R., Specht C.D., Rothfels C.J. 2022.
888 Unearthing modes of climatic adaptation in underground storage organs across Liliales.
889 bioRxiv.:2021.09.03.458928.

890 Uyeda J.C., Harmon L.J. 2014. A novel Bayesian method for inferring and interpreting the
891 dynamics of adaptive landscapes from phylogenetic comparative data. Systematic
892 biology. 63:902–918.

893 Uyeda J.C., Zenil-Ferguson R., Pennell M.W. 2018. Rethinking phylogenetic comparative
894 methods. Syst Biol. 67:1091–1109.

895 Vasconcelos, T., Boyko, J. D., & Beaulieu, J. M. (2021). Linking mode of seed dispersal and
896 climatic niche evolution in flowering plants. Journal of Biogeography.

897 Vasconcelos T., O'Meara B.C., Beaulieu J.M. 2022. A flexible method for estimating tip
898 diversification rates across a range of speciation and extinction scenarios. Evolution.

899 Venable D.L., Brown J.S. 1988. The Selective Interactions of Dispersal, Dormancy, and Seed
900 Size as Adaptations for Reducing Risk in Variable Environments. The American
901 Naturalist. 131:360–384.

902 Westoby M., Leishman M., Lord J. 1996. Comparative ecology of seed size and dispersal.
903 Philosophical Transactions of the Royal Society of London. Series B: Biological
904 Sciences. 351:1309–1318.

905 Yang Z. 2006. Computational molecular evolution. Oxford University Press Oxford.

Supplementary Tables

Table S1. AIC weights summarizing the average support for each model class when they are the generating model. Data is generated with $q_{ij} = 0.1, \alpha_1 = 3, \alpha_2 = 1.5, \sigma_1^2 = 0.35, \sigma_2^2 = 1, \theta_1 = 2,$ and $\theta_2 = 0.75$ for phylogenies with 25, 100, and 250 taxa and model fits using either 25, 100, or 250 stochastic maps per likelihood iteration. When the generating model class is character dependent (CD) or character independent (CID+) we expect that the AICwt will be highest for that model when fit. Character dependent models generally show that pattern, however CID+ models generally perform poorly. An additional concern is datasets simulated by a character independent model with rate heterogeneity (datasets generated by a CID+ model) are best fit by CD models – which would be a spurious correlation. Although there was often some signal of character dependence in these models (AICwt of CD when CID+ is generating), most of the AIC weight was for simple character independent models (BM1 or OU1).

Generating model class	Generating model type	AICwt of BM1	AICwt of OU1	AICwt of CD	AICwt of CID+	Proportion generating model chosen as best
CD	BMV	0.18	0.17	**0.64**	0.02	0.62
	OUV	0.03	0.22	**0.74**	0.02	0.73
	OUA	0.07	**0.56**	0.31	0.06	0.15
	OUM	0.04	0.02	**0.9**	0.04	0.92
	OUVA	0.04	0.21	**0.7**	0.06	0.7
	OUMV	0.02	0.02	**0.93**	0.03	0.95
	OUMA	0.12	0.15	**0.64**	0.09	0.66
	OUMVA	0.05	0.13	**0.76**	0.06	0.76
	OUBM1	0.19	**0.58**	0.13	0.10	0.08
	OUBMV	0.07	0.20	**0.71**	0.02	0.73
CID+	BMV	**0.36**	0.28	0.33	0.03	0.01
	OUV	0.04	**0.49**	0.43	0.04	0.01
	OUA	0.06	**0.56**	0.37	0.02	0
	OUM	0.21	0.09	0.03	**0.67**	0.71
	OUVA	0.07	**0.55**	0.35	0.04	0.03
	OUMV	0.24	0.19	0.14	**0.44**	0.44
	OUMA	**0.41**	0.40	0.13	0.06	0.06
	OUMVA	0.24	**0.39**	0.21	0.16	0.15
	OUBM1	0.24	**0.55**	0.16	0.05	0.01
	OUBMV	0.23	**0.37**	0.30	0.10	0.08

Table S2: Modeling results from the 25 models fit to Ericaceae aridity index and fruit type data. Model classes are character independent without rate heterogeneity (CID), character dependence (CD), character independence with rate heterogeneity (CID+), and mixed character dependent and character independence (HYB). Character dependent models suggest that climatic niche evolution will be linked to the fruit type. We found substantial support for OUVA (variable σ^2 and α) and OUMVA (variable σ^2, α, and θ) models. np is the number of freely estimated parameters. lnLik is the joint likelihood of the MLE. DiscLik and ContLik are the marginal likelihood of the discrete and continuous datasets respectively, given the maximum joint likelihood estimate of the parameters. AIC is the Akaike information criterion, ΔAIC is the difference from the best fit model measured as the difference between each model's AIC, and AICwt is the relative support for each model.

Model class	Model type	np	lnLik	DiscLik	ContLik	AIC	ΔAIC	AICwt
CID	BM1	4	-243.89	-32.62	-206.67	495.78	39.07	0
	OU1	5	-225.5	-32.62	-188.28	461.01	4.30	0.05
CD	BMV	5	-243.78	-32.62	-207.08	497.56	40.85	0
	OUV	6	-225.49	-32.62	-188.47	462.98	6.27	0.02
	OUA	6	-224.95	-32.58	-189.48	461.9	5.19	0.03
	OUM	6	-224.12	-32.57	-187.79	460.24	3.53	0.07
	OUVA	***7***	***-221.62***	***-32.58***	***-184.44***	***457.24***	***0.53***	***0.32***
	OUMV	7	-224.05	-32.62	-188.15	462.10	5.39	0.03
	OUMA	7	-223.21	-32.58	-187.97	460.42	3.71	0.06
	OUMVA	***8***	***-220.35***	***-32.60***	***-183.27***	***456.71***	***0***	***0.41***
	OUBM1	5	-243.84	-32.57	-206.67	497.68	40.97	0
	OUBMV	6	-243.79	-32.61	-206.99	499.57	42.87	0
CID+	BMV	7	-244.80	-33.11	-205.78	503.59	46.89	0
	OUV	8	-228.77	-32.98	-190.16	473.55	16.84	0
	OUA	8	-226.42	-33.17	-188.53	468.84	12.13	0
	OUM	8	-226.43	-33.32	-189.07	468.87	12.16	0
	OUVA	9	-244.38	-33.43	-202.12	506.76	50.05	0
	OUMV	9	-225.20	-33.39	-182.88	468.39	11.68	0
	OUMA	9	-225.57	-32.68	-189.92	469.14	12.43	0
	OUMVA	10	-227.39	-33.13	-185.15	474.79	18.08	0
	OUBM1	7	-244.44	-33.16	-206.67	502.88	46.17	0
	OUBMV	8	-225.58	-32.71	-186.58	467.17	10.46	0
HYB	BMS	9	-244.46	-33.08	-204.83	506.93	50.22	0
	OUM	10	-224.12	-32.67	-188.99	468.23	11.52	0
	OUMVA	16	-226.56	-33.03	-179.11	485.13	28.42	0

Supplementary Figures

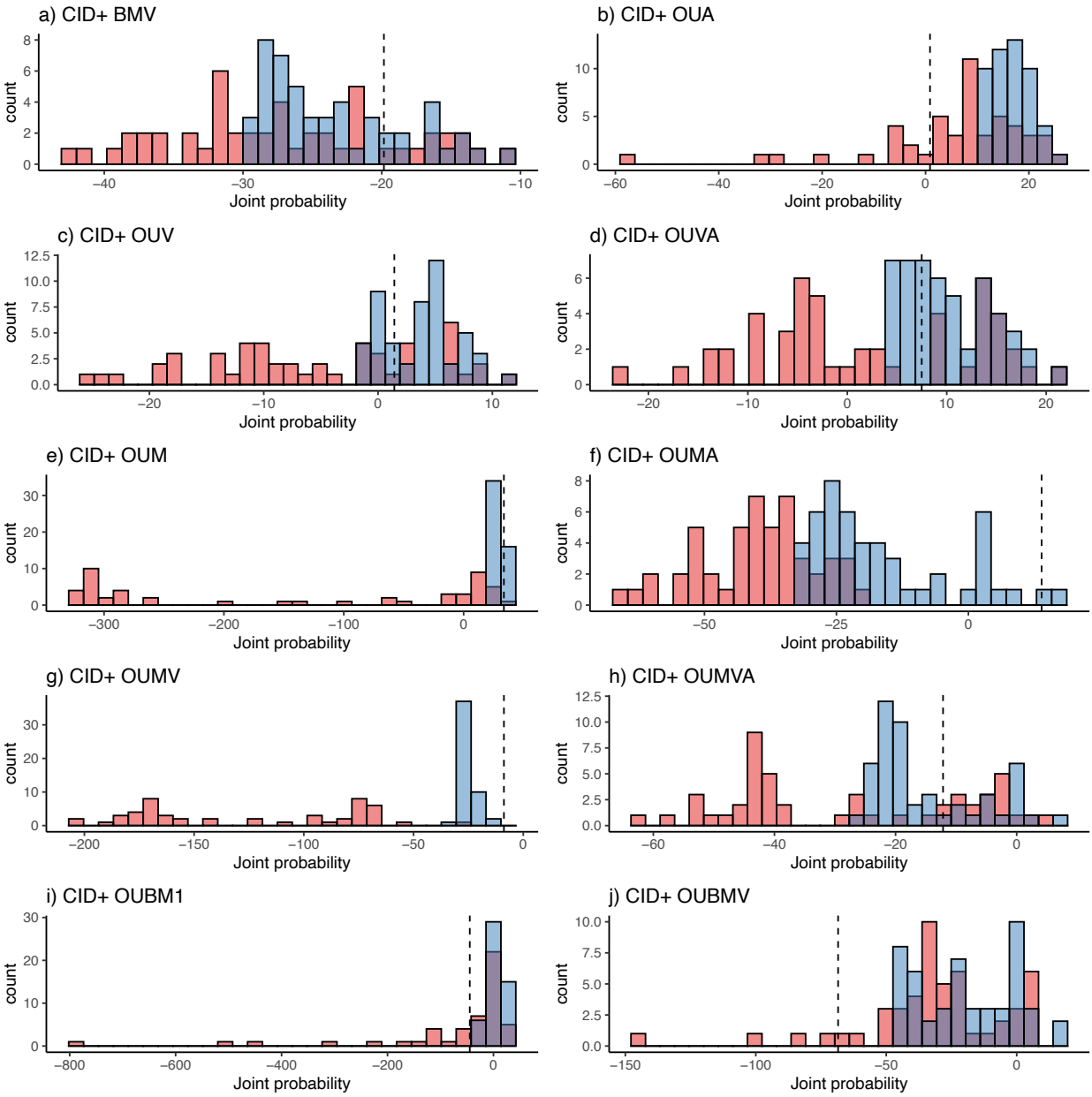

Figure S1. Overlapping histograms comparing the effectiveness of the adaptive sampling procedure (blue) and standard discrete only sampling (red) of maps. Regardless of the sampling procedure, all probabilities are calculated in the same way and so any differences in probabilities reflects each procedure's ability to generate appropriate mappings. 50 stochastic mappings are used to calculate the likelihood of the parameters. For each model type, data are simulated following our methods with $q_{ij} = 0.1, \alpha_1 = 3, \alpha_2 = 1.5, \sigma_1^2 = 0.35, \sigma_2^2 = 1, \theta_1 = 2,$ and $\theta_2 = 0.75$. Dashed line likelihood under generating map.

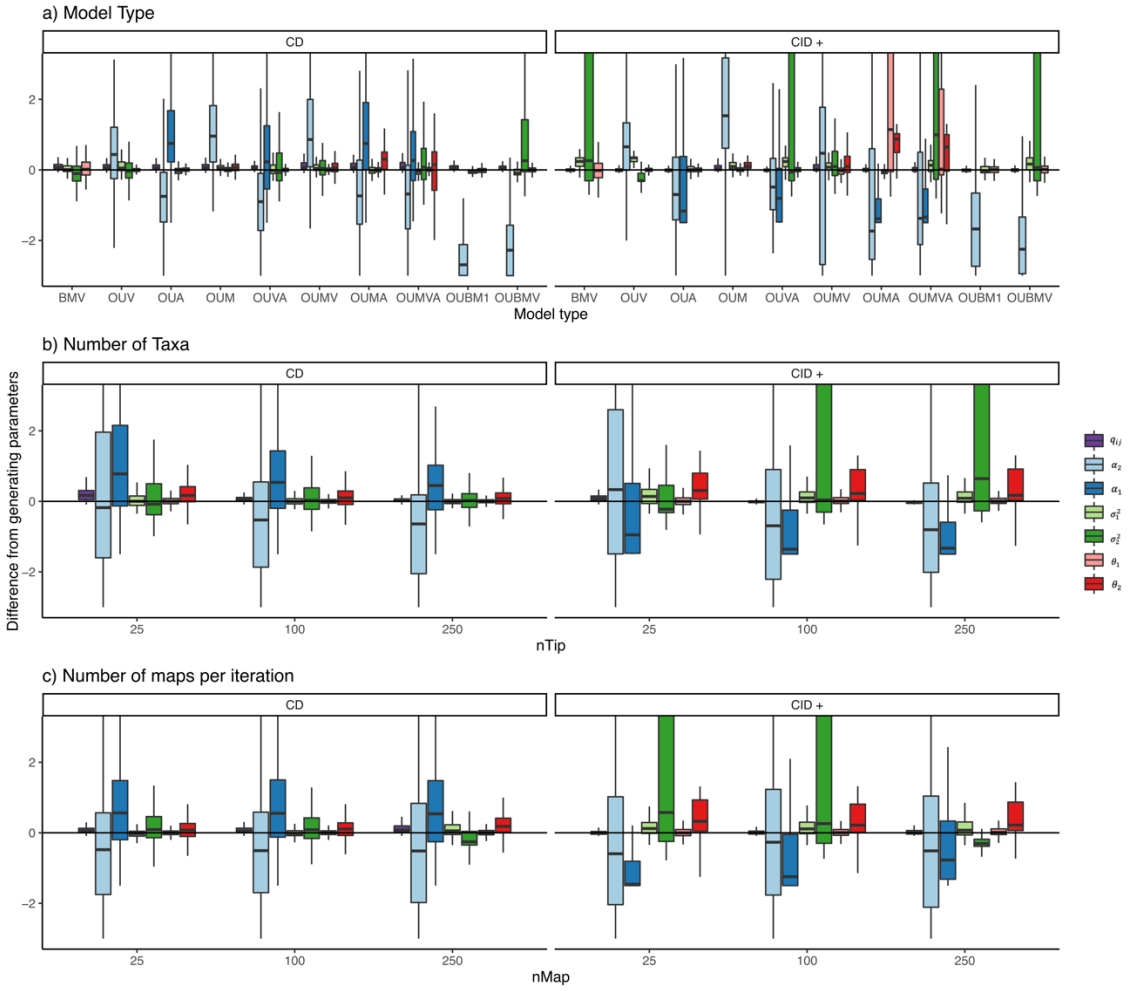

Figure S2. The raw difference of the maximum likelihood parameter estimates and the generating values depending on the a) model type, b) number of taxa in the dataset, and c) number of stochastic maps per iteration of the likelihood search. Generally, variable alpha models had the highest biases with alpha being consistently underestimated. As the number of taxa increased, estimation of CD model parameters was estimated with less error. The number of maps per iteration had the greatest effect on character independent models with rate heterogeneity.

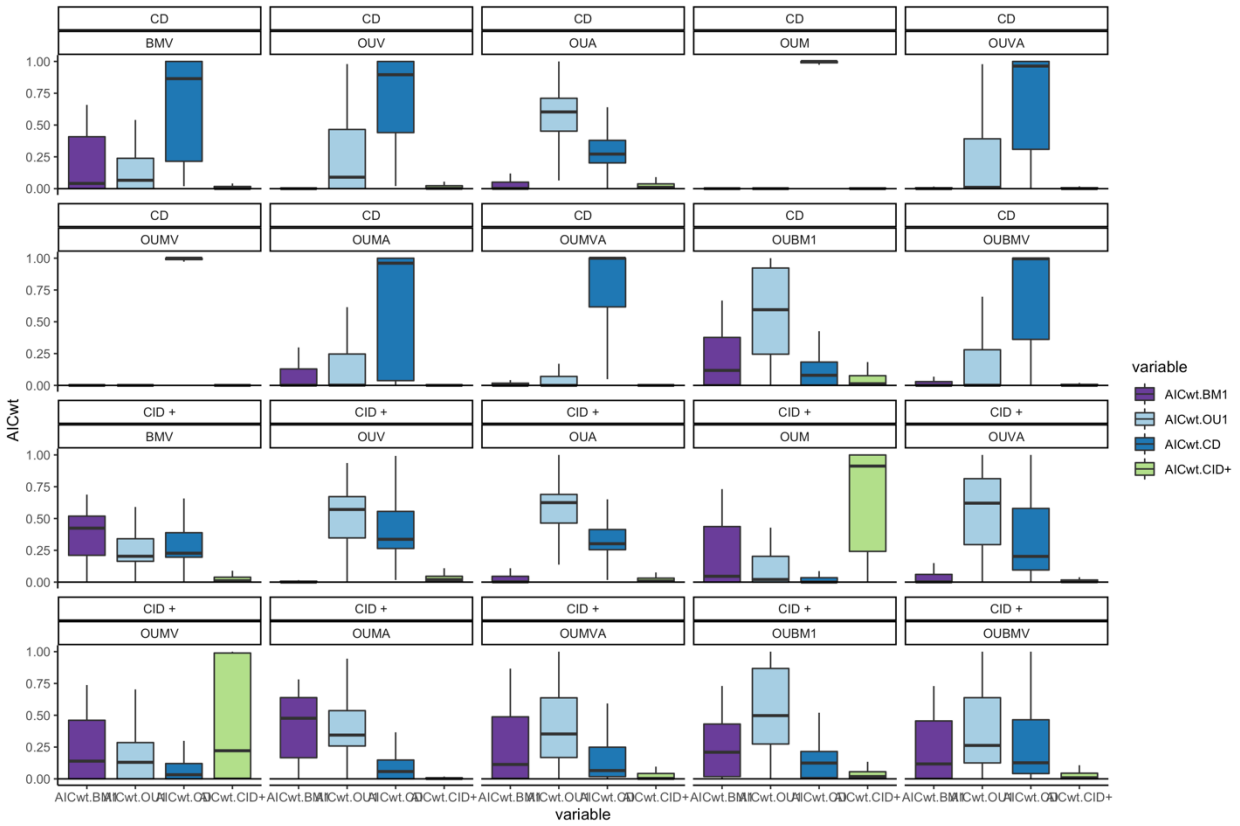

Figure S3. AIC weights summarizing the average support for particular model classes and model type when they are the generating model. Headings indicate the generating model type and model class. Data was generated with $q_{ij} = 0.1, \alpha_1 = 3, \alpha_2 = 1.5, \sigma_1^2 = 0.35, \sigma_2^2 = 1, \theta_1 = 2$, and $\theta_2 = 0.75$ for phylogenies with 25, 100, and 250 taxa and model fits using either 25, 100, or 250 stochastic maps per likelihood iteration. When the generating model class is character dependent (CD) or character independent (CID+) we expect that the AICwt will be highest for that model when fit.